Dynamical renormalization group study for a class of non-local interface equations

J. Stat. Mech. (2011) P10030

(http://iopscience.iop.org/1742-5468/2011/10/P10030)

Journal of Statistical Mechanics: Theory and Experiment
An IOP and SISSA journal

Dynamical renormalization group study for a class of non-local interface equations

Matteo Nicoli[1], **Rodolfo Cuerno**[2] **and Mario Castro**[3]

[1] Physique de la Matière Condensée, École Polytechnique, CNRS, 91128 Palaiseau, France
[2] Departamento de Matemáticas and Grupo Interdisciplinar de Sistemas Complejos (GISC), Universidad Carlos III de Madrid, Avenida de la Universidad 30, 28911 Leganés, Spain
[3] GISC and Grupo de Dinámica No Lineal (DNL), Escuela Técnica Superior de Ingeniería (ICAI), Universidad Pontificia Comillas, 28015 Madrid, Spain
E-mail: matteo.nicoli@polytechnique.edu, cuerno@math.uc3m.es and marioc@upcomillas.es

Received 28 July 2011
Accepted 3 October 2011
Published 31 October 2011

Online at stacks.iop.org/JSTAT/2011/P10030
doi:10.1088/1742-5468/2011/10/P10030

Abstract. We provide a detailed dynamic renormalization group study for a class of stochastic equations that describe non-conserved interface growth mediated by non-local interactions. We consider explicitly both the morphologically stable case, and the less studied case in which pattern formation occurs, for which flat surfaces are linearly unstable to periodic perturbations. We show that the latter leads to non-trivial scaling behavior in an appropriate parameter range when combined with the Kardar–Parisi–Zhang (KPZ) nonlinearity, which nevertheless does not correspond to the KPZ universality class. This novel asymptotic behavior is characterized by two scaling laws that fix the critical exponents to dimension-independent values, which agree with previous reports from numerical simulations and experimental systems. We show that the precise form of the linear stabilizing terms does not modify the hydrodynamic behavior of these equations. One of the scaling laws, usually associated with Galilean invariance, is shown to derive from a vertex cancellation that occurs (at least to one loop order) for any choice of linear terms in the equation of motion and is independent of the morphological stability of the surface, hence generalizing this well-known property of the KPZ equation.

1742-5468/11/P10030+42$33.00

Moreover, the argument carries over to other systems such as the Lai–Das Sarma–Villain equation, in which vertex cancellation is known *not to* imply an associated symmetry of the equation.

Keywords: growth instabilities (theory), kinetic roughening (theory), self-affine roughness (theory)

Contents

1. Introduction

Many surface growth systems can be described by stochastic differential equations that capture the evolution of the surface height $h(\mathbf{r}, t)$ at time t and point $\mathbf{r}$ on a d-dimensional substrate [1, 2]. In many cases these equations are derived from first principles [3, 4], thus linking the small-scale physics of the growth process with a coarse-grained description of the surface height. Sometimes, this procedure ends up expressing a physical problem in which interactions are short-range and local, into a stochastic equation in which *effective* interactions turn out to be long-range and/or non-local due to kinetic constraints. An example is provided by diffusion-limited growth [5, 6] (or erosion [7]) of an aggregate,

J. Stat. Mech. (2011) P10030

in which the local growth velocity depends on the global morphology of the evolving cluster, due to shadowing effects produced by the most prominent surface peaks over less exposed areas. Thus, a local transport mechanism such as diffusion induces long-range correlations among positions at the aggregate surface. Dynamically, this may result in a morphological instability in the case of a growing surface (protuberances *grow* faster, amplifying deviations from a flat interface), or morphological stability in the case of an eroding one (protuberances *decay* faster so that deviations from a flat interface are attenuated).

In principle, the non-local morphologically unstable case is more interesting than the non-local morphologically stable case, since the latter is known to lead to trivial scaling behavior, in the sense that the corresponding scaling exponents can be obtained from simple dimensional analysis as applied to the corresponding linearized equation [7, 8]. On the other hand, morphological instabilities are key to pattern-forming systems [9], *non-local* linear instabilities having been the subject of extensive studies in the past. Celebrated examples include the Mullins–Sekerka (MS) instability in solidification [10], the Saffman–Taylor (ST) hydrodynamic instability in fluid flow [11, 12], or the Darrieus–Landau (DL) instability [13]–[16] occurring in the propagation of a premixed laminar flame, to cite a few.

The stochastic equations that describe morphologically unstable surfaces typically combine linear terms that account for the selection of a typical wavelength associated with that among the height field modes, $h_{\mathbf{k}}(t) = \mathcal{F}[h(\mathbf{r}, t)]_{\mathbf{k}}$, that has the largest growth rate [9], with additional nonlinear terms that stabilize the exponential growth due to the morphological instability, and prevent blow up the surface height field. Here, $\mathcal{F}$ stands for the space Fourier transform and $\mathbf{k}$ is a wavevector. In the context of surface growth, the Kardar–Parisi–Zhang (KPZ) [17] nonlinearity $(\nabla h)^2$ is expected whenever the interface evolves in the absence of conservation laws [2, 18]. Thus, a natural example for a model of unstable surface growth subject to external fluctuations is given for example by

$$\partial_t h = \nu \nabla^2 h - \mathcal{K} \nabla^4 h + \frac{\lambda}{2} (\nabla h)^2 + \eta, \tag{1}$$

where η is an uncorrelated Gaussian noise with zero mean and constant variance $2\Pi_0$, i.e.,

$$\langle \eta(\mathbf{x}, t) \eta(\mathbf{x}', t') \rangle = 2\Pi_0 \, \delta(\mathbf{x} - \mathbf{x}') \, \delta(t - t'). \tag{2}$$

In equation (1), $\nu < 0$, $\mathcal{K} > 0$, and λ are parameters. A *negative* value for ν implements the morphological instability, which is countered both by the biharmonic and by the nonlinear terms. Equation (1) is the noisy Kuramoto–Sivashinsky (nKS) equation [4], whose deterministic limit is a paradigmatic model for chaotic spatially extended systems, arising in a variety of physical contexts, such as thin solid films, interfaces between viscous fluids, waves in plasmas and chemical reactions, reaction–diffusion systems, and others [9]. Actually, the large-scale behavior of the nKS systems is in the KPZ universality class both in one and in two spatial dimensions [19]–[23]. This is a remarkable manifestation of renormalization, by which the 'surface tension' parameter ν flows from a bare *negative* value to a positive renormalized value at large scales, as initially conjectured by Yakhot thirty years ago [24].

doi:10.1088/1742-5468/2011/10/P10030

J. Stat. Mech. (2011) P10030

Indeed, the KPZ (or noisy Burgers [25]) equation reads

$$\partial_t h = \nu\nabla^2 h + \frac{\lambda}{2}(\nabla h)^2 + \eta, \tag{3}$$

where $\nu > 0$. The KPZ nonlinear term is invariant under translations in the growth direction ($h \to h + c$, with c an arbitrary constant), in the substrate direction ($x \to x + a$) and, besides, it is symmetric under rotations and inversion about the growth direction [1]. Its ubiquity has led to a huge amount of work in the past, the KPZ equation having become one of the central problems in non-equilibrium interface dynamics [1, 2, 26]. Actually, based on dynamical renormalization group (DRG) arguments [17, 27], KPZ scaling is generically expected at the asymptotic state for non-conserved growth systems. However, such a theoretical expectation has been too scarcely confirmed by experiments [28]. One possible explanation is that short-time morphological instabilities (of the type occurring e.g. in the noisy Kuramoto–Sivashinsky system) may hinder the observation of the asymptotic behavior [5]. For instance, for appropriate choices of parameter values in the nKS equation, KPZ scaling may become unobservable even in numerical simulations [22]. Moreover, some of the hypothesis made in the derivation of the KPZ equation may not be realistic for many experimental situations. In particular, complex processes may take place in the system, such as diffusion, advection in a fluid, elastic stress in the aggregate, etc that break down the assumption of *local* interactions.

Following the above ideas, a number of non-local versions of the KPZ equation have been proposed—see e.g. [29]–[31] and further references in [28]—in order to account for scaling exponent values seen in experimental conditions that differ from the KPZ values. However, some of these are ad hoc generalizations that lack a clear physical justification. Moreover, most of them consider the morphologically stable condition (e.g., $\nu > 0$ in equations (1) and (3)), which, for uncorrelated time-dependent noise, leads to the scaling behavior associated with linear equations as mentioned above.

1.1. A family of non-local interface equations

There are other ways to generalize interface equations that do have a consistent physical interpretation. For instance, one can generate additional terms on the rhs of, say, equations (1) and (3), if one enforces full compatibility of the equation with the symmetries of the system [18]. Otherwise, starting from a first-principles formulation of a specific growth system in terms of, e.g., a moving boundary problem, one can derive explicitly the evolution equation for $h(\mathbf{r}, t)$ through projection of the whole bulk dynamics onto the interface, under suitable approximations. For non-conserved diffusion-limited growth, this has been accomplished for instance in [6, 32]. For epitaxial growth systems, see the review in [4]. Working along these lines, we have recently identified a whole family of non-local equations that is formulated as a single stochastic differential equation [33]. This equation has many relevant, well-known physical systems as particular cases. In Fourier space, the equation takes the simple form

$$\partial_t h_{\mathbf{k}}(t) = (-\nu k^\mu - \mathcal{K}k^m - \mathcal{N}k^n)h_{\mathbf{k}}(t) + \frac{\lambda}{2}\mathcal{F}[(\nabla h)^2]_{\mathbf{k}} + \eta_{\mathbf{k}}(t), \tag{4}$$

where k denotes the magnitude of the d-dimensional wavenumber $\mathbf{k}$, and $\eta_{\mathbf{k}}(t) = \mathcal{F}[\eta(t)]_{\mathbf{k}}$, with η as in equation (2). Here, μ, m, n, $\mathcal{K}$, and $\mathcal{N}$ are *positive* parameters such that

J. Stat. Mech. (2011) P10030

$0 < \mu \leq 2$, $m \geq 2$, and $n > m$, see below. We will consider both the morphologically unstable case in which $\nu < 0$, as in e.g. the noisy Kuramoto–Sivashinsky system, and the morphologically stable case $\nu > 0$. The term with coefficient $\mathcal{N}$ represents higher order stabilizing mechanisms that are required to make sense of parameter choices in which fluctuations do not dissipate at small scales, i.e. $-\nu k^{\mu} - \mathcal{K} k^{m} \to +\infty$ for $k \to +\infty$, as in the $\mu \to m = 2$ nKS-type limit. Still, one of the results of the present work is to explicitly prove the irrelevance of the term with coefficient $\mathcal{N}$ for the asymptotic scaling. Note that, whenever μ is *not* an even integer, the corresponding linear term in equation (4) is a fractional Laplacian acting on the height field,

$$(-\nabla^2)^{\mu/2} h(\mathbf{r}) = c_{d,\mu}\, \mathrm{PV} \int_{\mathbb{R}^d} \frac{h(\mathbf{r}) - h(\mathbf{r}')}{|\mathbf{r} - \mathbf{r}'|^{d+\mu}}\, \mathrm{d}\mathbf{r}', \qquad 0 < \mu \leq 2, \tag{5}$$

where PV denotes Cauchy principal value and $c_{d,\mu}$ are appropriate numerical constants [34, 35]. The Fourier representation of (5) is given by

$$\mathcal{F}[(-\nabla^2)^{\mu/2} h] = k^{\mu} h_{\mathbf{k}}. \tag{6}$$

Indeed, only if μ is an even integer can (5) be inverse Fourier transformed to get a local operator in real space, as in the noisy Kuramoto–Sivashinsky case. Otherwise, the fractional Laplacian corresponds to convolution of height differences with an algebraically decaying kernel. In the context of equilibrium systems with long-range interactions, equation (5) corresponds to the so-called 'weak' form of the latter, see [36] for a review. For the morphologically stable case, relaxation operators with the same shape as (5) have also been advocated to account for long-range interactions in processes defined both on Euclidean and on fractal lattices, see e.g. [2, 31, 37] and references therein.

For the morphologically unstable case, the linear dispersion relation that appears in equation (4), $\sigma_{\mathbf{k}} = -\nu k^{\mu} - \mathcal{K} k^{m}$, is common to many celebrated pattern-forming systems. Thus, for $\mu = 1$ and $m = 3$ we get the Mullins–Sekerka or Saffman–Taylor dispersion relations, while the Darrieus–Landau and Kuramoto–Sivashinsky cases are obtained for $\mu = 1$, $m = 2$, or for $\mu = 2$, $m = 4$, respectively. Thus, (4) allows us to study a large class of models in which a non-local morphological instability is coupled with the KPZ nonlinearity, which includes a number of equations that are important in their own rights, but also local models such as the nKS equation that have been exhaustively studied in the literature.

Apart from the noisy Kuramoto–Sivashinsky equation, we have the stochastic generalization of the Michelson–Sivashinsky (sMS) equation [38, 39] for $\mu = 1$, $m = 2$, which provides a standard model to describe propagation of premixed laminar flames [16]. Moreover, the sMS equation is the small slope approximation of a nonlinear equation found for growing interfaces controlled by *ballistic* transport [40], and has been also derived from first principles for reactive infiltration in porous media [41]. Likewise, an interface equation that we term MSKPZ, in which the Mullins–Sekerka dispersion relation ($\mu = 1$, $m = 3$) is combined with the KPZ nonlinearity, describes thin film growth by chemical vapor deposition (CVD) or by electrochemical deposition (in galvanostatic conditions) [6] when the attachment kinetics of aggregating particles is fast compared to the mean velocity of the growing interface, and has been recently employed to quantitatively describe CVD experiments [42]. Moreover, the linear dispersion relation appearing in (4) has been found to provide a phenomenological description for experimental systems in which transport is of a diffusive nature, using μ as a fitting parameter [43].

J. Stat. Mech. (2011) P10030

In [33], a numerical study has been reported for the family of equations (4) in one and two dimensions, together with a preliminary DRG study for fixed $m = 2$ as a representative case. Particular attention was paid to the morphologically unstable case $\nu < 0$ for which, strikingly, non-trivial (nonlinear) scaling occurs. Thus, under such conditions, simulations suggest that, for each dimension d, the universality class changes at $\mu = z_{\rm KPZ}(d)$. Unstable equations characterized by μ, such that $z_{\rm KPZ}(d) \leq \mu \leq 2$, are all in the KPZ universality class (as for the noisy Kuramoto–Sivashinsky equation), while the scaling behavior for small values $0 < \mu < z_{\rm KPZ}(d)$ is characterized by dimension-independent exponents that are *different* from those predicted by dimensional analysis. Here, $z_{\rm KPZ}(d)$ denotes the dynamic exponent of the KPZ class for the given value of d. For the definition of the critical exponents in these systems, see section 2.

In the present work, we perform a detailed DRG study of (4) for arbitrary substrate dimensions and considering both the morphologically stable and unstable conditions. Although the perturbative DRG has well-known limitations [25, 26], it has recently shown a remarkable explanatory power for various types of systems that include conserved or non-conserved versions of the KPZ nonlinearity, under morphologically stable (see [44, 45] and references therein) or unstable [46] conditions. We expect relevant information to be also obtained from the DRG flow on the asymptotic properties of equation (4). Indeed, our present work extends previous analytical results in a number of important aspects: (i) by generalizing the linear dispersion relation and the nonlinearity appearing in the stochastic equation to more general forms, we prove that a vertex cancellation occurs to one loop order in our perturbative expansion, inducing a Galilean scaling relation at the nonlinear fixed points found in the numerical simulations of [33]. The ensuing equation generalizes both the KPZ and the Lai–Das Sarma–Villain [47, 48] equations. Thus, explicit symmetry under a Galilean transformation, which occurs for the former equation but not for the latter, is seen not to be a necessary condition for the mentioned scaling relation to apply. Moreover, this scaling relation also holds at the asymptotic state numerically characterized for sufficiently small μ values in the morphologically unstable case of equation (4). (ii) We consider in detail the RG flow for arbitrary d, obtaining fixed points and flow properties that remained unexplored in [33]. In particular, we assess in detail the extent to which the renormalization flow of (4) inherits the structure of the perturbative KPZ flow. (iii) Working on the reference $m = 2$ case for $\mu = 1$, we prove explicitly that the additional interactions $-\mathcal{N}k^n h_{\mathbf{k}}$ do not modify the asymptotic behavior for $n = 3, 4$; this justifies numerical results in [33] that exploited this fact and had remained analytically unproven thus far. As a bonus, this result also justifies our parameter restriction to the case $\mu \leq 2$ in the definition of equation (4), since taking $\mu > 2$ in the equation generates $k^2 h_{\mathbf{k}}$ terms under renormalization that become more relevant than the bare $k^\mu h_{\mathbf{k}}$ ones.

The paper is organized as follows: as a preliminary, we start in section 2 with a scaling analysis of the family of equations (4) through power counting and through a more refined Flory-type approach [49], and with considerations on their naive upper critical dimensions. Given the insufficiency of mere scaling analysis, in section 3 we outline the perturbative DRG procedure as applied to equation (4). We provide the proof on the mentioned vertex cancellation leading to the Galilean scaling relation. In section 4 we discuss the most convenient parameter space in which to study the DRG flow. This is addressed in detail in section 5, where we provide the main results (fixed points, stability and critical

J. Stat. Mech. (2011) P10030

exponents) for dimensions $d = 1$, $d = 2$, and $d > 2$, assessing how dimensionality changes the overall properties of the equation. Finally, in section 6, we discuss the significance of our results, both for the equations studied and from a more general perspective for surface kinetic roughening, and give our conclusions and an outlook. In order to make our presentation self-contained while trying not to obscure it, a number of technical details are provided in appendices.

2. Scaling analysis and upper critical dimension

In order to gain some intuition into the scaling behavior that can be expected for equation (4), we can perform a scaling analysis. Straightforward power counting first leads to the conclusion that, under a rescaling of the height field and space and time coordinates as $\tilde{h}(\mathbf{r}, t) = b^{-\alpha} h(b\mathbf{r}, b^z)$ with $b > 1$, an equation with the same shape as (4) holds for $\tilde{h}$, with rescaled parameters

$$\tilde{\nu} = b^{z-\mu}\nu, \qquad \tilde{\mathcal{K}} = b^{z-m}\mathcal{K}, \qquad \tilde{\lambda} = b^{\alpha+z-2}\lambda, \qquad \tilde{\Pi}_0 = b^{z-2\alpha-d}\Pi_0. \tag{7}$$

Here, α and z are, respectively, the roughness and dynamic exponents that characterize the scaling behavior of the system. The behavior of the ratio $\tilde{\mathcal{K}}/\tilde{\nu}$ immediately implies that $\mathcal{K}$ is less relevant than ν under rescaling, since $\mu < m$. Likewise, under morphologically stable conditions, we expect $\alpha < 1$, leading to the dominance of the non-local term over the KPZ term for $\mu \leq 1$. Conversely, for morphologically unstable conditions we can assume $\alpha > 1$, so that we would expect ν to be irrelevant as compared with λ for $\mu \geq 1$.

Power counting is indeed limited in its predictions regarding precise values of scaling exponents and expected behavior outside the exponent regions considered in the previous paragraph. One can improve over these results by performing a scaling argument à la Flory [49] in which one estimates the magnitude of individual terms present in (4). We assume that at long times $t \gg t_l$, and averaged over length scales l, the height–height correlation function [1] scales as $C(l, t) \sim h_l^2 \sim l^{2\alpha}$, and that at long times the relaxation time of these fluctuations is $t_l \sim l^z$. Note that t_l and h_l depend on the length scale l. The various terms in equation (4) can be estimated as

$$\langle|\partial_t h|\rangle_l \sim \frac{h_l}{t_l}, \qquad \nu \left\langle \left|\mathcal{F}^{-1}[k^\mu h_{\mathbf{k}}]\right| \right\rangle_l \sim \nu \frac{h_l}{l^\mu}, \qquad \lambda \left\langle \left|(\nabla h)^2\right| \right\rangle_l \sim \lambda \frac{h_l^2}{l^2}. \tag{8}$$

For white noise we can estimate its mean-square fluctuations on length scales l and time scales t_l as $\eta_l \sim (\Pi_0/S_l t_l)^{1/2}$, where S_l is the average surface area of the interface on scale l, and thus $S_l \sim (h_l^2 + l^2)^{d/2}$ [49]. For morphologically stable conditions, the l^2 term in S_l dominates the height fluctuations (namely, $\alpha < 1$); instead, for morphologically unstable surfaces the dominant term is h_l^2. Let us start by considering the former case, and assume that ν dominates over λ. Then, by equating the non-local term with the inertial term (the one proportional to the time derivative of h), we obtain a simple condition for the characteristic time of the height fluctuations $t_l \sim l^\mu/\nu$ and, consequently, the relation $z = \mu$. Under these conditions we estimate $\eta_l \sim (\Pi_0/l^d t_l)^{1/2}$, and equating in turn the inertial term with the noise fluctuations we obtain $h_l \sim l^{(\mu-d)/2}$. This expression gives us the value of the roughness exponent $\alpha = (\mu - d)/2$, which combined with $z = \mu$ leads to the so-called hyperscaling relation $2\alpha + d = z$, see section 4. This set of exponents has indeed been observed in our numerical simulations of the morphologically stable condition [33]. In

J. Stat. Mech. (2011) P10030

the morphologically unstable case, we expect the noise term to scale as $\eta_l \sim (\Pi_0/h_l^d t_l)^{1/2}$. If we try to equate this with the inertial term, we expect a violation of hyperscaling. Led by the previous power counting analysis, we now equate the inertial and KPZ terms, leading to $h_l \sim l^2 t_l^{-1} \sim l^{2-z} \sim l^{\alpha}$, i.e. we obtain the so-called Galilean exponent relation $\alpha + z = 2$.

In principle we have not assumed any restrictions on the values of μ when deriving the previous scaling relations and exponent values. As mentioned in section 1.1, numerical simulations of the morphologically unstable condition [33] indicate that the scaling behavior depends non-trivially on the precise value of μ. Moreover, the present argument does not allow us to assess possible changes for different substrate dimension d. For these reasons, we need to resort to more refined scaling analysis, among which the DRG is a natural choice.

Before leaving this section, we can also make estimates on the naive critical dimension of equation (4) by making use of equations (7). As in the standard KPZ case [50], the idea is to employ the exponents associated with the relevant linear theory in order to derive conditions under which $\tilde{\lambda}$ scales to zero, or else grows unboundedly for increasing b. Typically such conditions depend on the value of d, hence the appearance of a critical dimension. In our case, given that the linearized equation (4) blows up exponentially in time for the morphologically unstable condition, such an estimate can only be meaningful, if at all, in the morphologically stable condition. Thus, employing the exponent values $z = \mu$ and $\alpha = (z-d)/2$, we get $\tilde{\lambda} = b^{n_\lambda}\lambda$ with $n_\lambda = (3\mu-4-d)/2$. Hence, the nonlinearity becomes irrelevant for $d > d_c(\mu) = 3\mu - 4$, which is the case for $d \geq 2$ and any value of μ (note $d_c = 0$ for $\mu = 4/3$). Alternatively, this implies that in $d < 2$ dimensions there exists a critical value $\mu_c(d) = (4 + d)/3$ such that for $0 < \mu < \mu_c(d)$ the critical exponents are again given by the linear equation (mean-field). For $\mu_c(d) < \mu < 2$ the scaling behavior should be controlled by the nonlinearity; we reconsider this result in section 5 below. In general, for $\mu \geq 2$ we expect also KPZ-type behavior, but that remains beyond power counting analysis, as it requires renormalization. Note the strong similarities between these results and those expected for equilibrium systems with so-called weak long-range interactions [36], in particular about the possibility that non-localities can modify the values of the critical exponents [51], and the occurrence of mean-field-type behavior as a function of μ.

3. Sketch of the renormalization procedure

Previous studies on the morphologically stable version of (4) (namely, $\nu > 0$) for $\mu = 1$ show that the equation indeed produces scale-invariant interfaces whose critical exponents follow from a simple dimensional analysis such as the one performed in section 2 [7]. Actually, under conditions of morphological stability, one can even obtain analytically the exponents for arbitrary μ values in the deterministic limit [8], which are expected to apply also for the stochastic case [30]. However, the behavior for the morphologically unstable cases has been studied only recently [33]. In that work we integrated equation (4) numerically using a pseudospectral scheme [52, 53] for $d = 1, 2$, and different values of μ. The exponents measured numerically were confirmed through a DRG analysis using the Forster–Nelson–Stephen (FNS) [54] scheme. In this section we sketch the general ideas of the latter approach, and show that the KPZ nonlinearity does not

J. Stat. Mech. (2011) P10030

renormalize for any linear dispersion relation that is a linear combination of arbitrary powers of the wavenumber k, a result that actually is independent of the morphological stability/instability of the system, i.e., on the sign of ν, and generalizes known results for the KPZ and Lai–Das Sarma–Villain equations.

For the sake of generality, it is convenient to consider the evolution equation for a generic linear dispersion relation $\sigma_{\mathbf{k}}$. Thus,

$$\partial_t h_{\mathbf{k}}(t) = \sigma_{\mathbf{k}} h_{\mathbf{k}}(t) + \frac{\lambda}{2}\mathcal{F}[(\nabla h)^2]_{\mathbf{k}} + \eta_{\mathbf{k}}(t), \tag{9}$$

where the noise term is as in equation (4). The DRG procedure starts by writing equation (9) after time Fourier transform,

$$[-\sigma_{\mathbf{k}} - \mathrm{i}\omega]\, h_{\mathbf{k},\omega} = \eta_{\mathbf{k},\omega} - \frac{\lambda}{2}\int_{|\mathbf{q}|\leq\Lambda}\frac{\mathrm{d}\mathbf{q}}{(2\pi)^d}\int_{-\infty}^{+\infty}\frac{\mathrm{d}\Omega}{2\pi}\,\mathbf{q}\cdot(\mathbf{k}-\mathbf{q})\, h_{\mathbf{q},\Omega}\, h_{\mathbf{k}-\mathbf{q},\omega-\Omega}, \tag{10}$$

where ω is the time frequency, $\Lambda = \pi/\Delta x$ is the wavenumber cut-off in the system, Δx being the lattice spacing in real space. In Fourier space, the noise term in (10) still has zero mean $\langle\eta_{\mathbf{k},\omega}\rangle = 0$ and is delta correlated, but its variance is rescaled by a constant as

$$\langle\eta_{\mathbf{k},\omega}\,\eta_{\mathbf{k}',\omega'}\rangle = 2\Pi_0(2\pi)^{d+1}\,\delta_{\mathbf{k}+\mathbf{k}'}\,\delta_{\omega+\omega'}. \tag{11}$$

Following the standard FNS procedure [25, 26, 54], the height and the noise fields are split into two types of component, slow modes $h^<_{\mathbf{k},\omega}$, $\eta^<_{\mathbf{k},\omega}$ for wavenumbers $0 < k < \Lambda/b$, and fast modes $h^>_{\mathbf{k},\omega}$, $\eta^>_{\mathbf{k},\omega}$ for $\Lambda/b \leq k \leq \Lambda$, where $b = \mathrm{e}^{\delta l}$ is a rescaling parameter (assumed to be larger than one, i.e. $\delta l > 0$). Then one eliminates a 'small number' (namely, δl is infinitesimal) of the fast modes by solving the growth equation perturbatively for $h^>_{\mathbf{k},\omega}$, substituting the solution into the equation for the slow modes and assuming statistical independence between high and low-frequency components. This procedure leads to an effective equation in which the fast modes are thus integrated out,

$$[-\sigma_{\mathbf{k}} - \Sigma(\mathbf{k},0) - \mathrm{i}\omega]\; h^<_{\mathbf{k},\omega} = \eta^<_{\mathbf{k},\omega} - \frac{\lambda}{2}\int_<\frac{\mathrm{d}\mathbf{q}}{(2\pi)^d}\int\frac{\mathrm{d}\Omega}{2\pi}\,\mathbf{q}\cdot(\mathbf{k}-\mathbf{q})\, h^<_{\mathbf{q},\Omega}\, h^<_{\mathbf{k}-\mathbf{q},\omega-\Omega} + \mathrm{O}(\lambda^3), \tag{12}$$

where the effect of this coarse-graining step (the elimination of fast modes) is obtained by solving perturbatively the following integral (for the result in a particular representative case of equation (4), see appendix A)

$$\begin{aligned}\Sigma(\mathbf{k},\omega) = 2\lambda^2\Pi_0\int_>\frac{\mathrm{d}\mathbf{q}}{(2\pi)^d}\int\frac{\mathrm{d}\Omega}{2\pi}\,[\mathbf{q}\cdot(\mathbf{k}-\mathbf{q})]\,[-\mathbf{q}\cdot\mathbf{k}] \\ \times\, G_0(\mathbf{q},\Omega)G_0(-\mathbf{q},-\Omega)G_0(\mathbf{k}-\mathbf{q},\omega-\Omega).\end{aligned} \tag{13}$$

In equations (12) and (13) we have denoted integrals over the fast (slow) modes with $\int_>$ ($\int_<$), and we have omitted the integration limits in the frequency domain (note that $\Omega \in (-\infty,\infty)$). In equation (13), $G_0(\mathbf{k},\omega) = [-\sigma_{\mathbf{k}} - \mathrm{i}\omega]^{-1}$ is the bare propagator, and the integral in $\mathbf{q}$ is calculated only for the (fast) modes within the *shell* $q \in [\Lambda/b, \Lambda]$. In equation (12) the coarse-grained propagator appears,

$$G^<_0(\mathbf{k},\omega) \equiv [-\sigma_{\mathbf{k}} - \Sigma(\mathbf{k},0) - \mathrm{i}\omega]^{-1}. \tag{14}$$

J. Stat. Mech. (2011) P10030

From this expression, the effect of coarse-graining on the propagator is seen to merely amount to a modification of the system parameters. For example, $\Sigma(\mathbf{k},0)=\Sigma_\nu k^\mu+\Sigma_\mathcal{K}k^2$ for equation (4) for $m=2$, so that the renormalized propagator has the same functional shape as the bare propagator, but with modified coefficients $\nu^<=\nu+\Sigma_\nu$ and $\mathcal{K}^<=\mathcal{K}+\Sigma_\mathcal{K}$. Actually, in equation (12) we have omitted higher order terms that can in principle be associated with a change in the value of $\lambda\to\lambda^<$, as induced by the present coarse-graining step, see section 3.1.

On the other hand, the coarse-graining of the noise variance is performed by starting from equation

$$\left\langle h^<_{\mathbf{k},\omega}h^<_{-\mathbf{k},-\omega}\right\rangle=2\Pi_0^<\,G(\mathbf{k},\omega)G(-\mathbf{k},-\omega), \tag{15}$$

in which the exact propagator appears. This equation leads, after a little algebra, to

$$\langle\eta^<_{\mathbf{k},\omega}\,\eta^<_{\mathbf{k}',\omega'}\rangle=2\left[\Pi_0+\Phi(\mathbf{k},0)\right](2\pi)^{d+1}\,\delta_{\mathbf{k}+\mathbf{k}'}\,\delta_{\omega+\omega'}+\mathrm{O}(\lambda^3), \tag{16}$$

where the coarse-grained noise variance is given by

$$\Phi(\mathbf{k},\omega)=\lambda^2\Pi_0^2\int_>\frac{\mathrm{d}\mathbf{q}}{(2\pi)^d}\int\frac{\mathrm{d}\Omega}{2\pi}\,[\mathbf{q}\cdot(\mathbf{k}-\mathbf{q})]^2|G_0(\mathbf{q},\Omega)|^2|G_0(\mathbf{k}-\mathbf{q},\omega-\Omega)|^2. \tag{17}$$

Hence, the noise variance in the equation for the slow modes is $\Pi_0^<=\Pi_0+\Phi$. For the result in a particular representative case of equation (4), see appendix A.

3.1. Vertex cancellation for generalized equations

In this section we show that, to within our one loop approximation, the coarse-graining procedure does *not* lead to a modification in the coefficient of the nonlinearity for equation (9) with quite general $\sigma_\mathbf{k}$, namely, $\lambda^<=\lambda$. Specifically, we consider any linear dispersion relation that can be written as

$$\sigma_\mathbf{k}=-\sum_{i=1}^n c_i|\mathbf{k}|^{r_i}, \tag{18}$$

where the set $\{r_i\}$ is formed by a collection of positive real exponents that increase with the index, $r_1<r_2<\cdots<r_n$, and coefficients c_i are generic, but with the restriction that c_n is positive in order to obtain a well-behaved dispersion relation at high wavenumbers, i.e. $\sigma_\mathbf{k}\to-\infty$ for $k\to\infty$. Given this choice, we consider an even more general equation of which (9) is a particular case, namely,

$$\partial_t h_\mathbf{k}(t)=\sigma_\mathbf{k}h_\mathbf{k}(t)-\frac{\lambda}{2}k^\sigma\mathcal{F}[(\nabla h)^2]_\mathbf{k}+\eta_\mathbf{k}(t), \tag{19}$$

where $\sigma\geq0$, see [55] for the special case in which $\sigma_\mathbf{k}=-\nu k^{\mu+\sigma}$. Note that equation (19) reduces to (9) for $\sigma=0$. In the same way as the latter includes the KPZ equation as a particular case, equation (19) generalizes also the celebrated Lai–Das Sarma–Villain equation [47, 48], which is obtained for $\mu=\sigma=2$. In short, the latter is a conserved version of the KPZ equation with non-conserved noise, and has played an important role in the study of kinetic roughening for thin films grown by MBE [2].

As is well known and is reviewed in detail elsewhere [25, 26], the iterative solution of equations like (10) or (19) along the lines sketched above can be conveniently cast

J. Stat. Mech. (2011) P10030

into a diagrammatic formulation (for notation and diagrams, see e.g. [27]). Within such scheme, it is seen that the coarse-graining process is complete at one loop order once the coarse-grained coupling $\lambda^<$ of the nonlinear term is evaluated from

$$
\begin{aligned}
-\frac{\lambda}{2}^{<} k_1^{\sigma} \int_{>} \frac{\mathrm{d}\mathbf{k}_2}{(2\pi)^d} \int \frac{\mathrm{d}\Omega_2}{2\pi} \left(\frac{\mathbf{k}_1}{2}+\mathbf{k}_2\right)\cdot\left(\frac{\mathbf{k}_1}{2}-\mathbf{k}_2\right) h^{<}_{\mathbf{k}_1/2+\mathbf{k}_2,\omega_1/2+\Omega_2}\, h^{<}_{\mathbf{k}_1/2-\mathbf{k}_2,\omega_1/2-\Omega_2} \\
\equiv -\frac{\lambda}{2} k_1^{\sigma} \int_{>} \frac{\mathrm{d}\mathbf{k}_2}{(2\pi)^d} \int \frac{\mathrm{d}\Omega_2}{2\pi} \left(1+\sum_{j=1}^{3}\Gamma_j\right) \\
\times \left(\frac{\mathbf{k}_1}{2}+\mathbf{k}_2\right)\cdot\left(\frac{\mathbf{k}_1}{2}-\mathbf{k}_2\right) h^{<}_{\mathbf{k}_1/2+\mathbf{k}_2,\omega_1/2+\Omega_2}\, h^{<}_{\mathbf{k}_1/2-\mathbf{k}_2,\omega_1/2-\Omega_2} + \mathrm{O}(\lambda^5), \qquad (20)
\end{aligned}
$$

where the original variables $\mathbf{k}$ and $\mathbf{q}$ in (10) are replaced by the symmetric variables $\mathbf{k}_1=\mathbf{k}$ and $\mathbf{k}_2=\mathbf{q}-\mathbf{k}/2$, and Γ_j are appropriate integrals that are evaluated next. The first one arises from the contraction of fast noise components with wavevectors $\pm((\mathbf{k}_1/2)+\mathbf{k}_2-\mathbf{q})$, and reads

$$
\begin{aligned}
\Gamma_1(\mathbf{k}_1,\mathbf{k}_2,\omega_1,\omega_2) = \frac{2\lambda^2\Pi_0}{((k_1^2/4)-k_2^2)} \int_{>} \frac{\mathrm{d}\mathbf{q}}{(2\pi)^d} \int \frac{\mathrm{d}\Omega}{2\pi} \left(q|\mathbf{k}_1-\mathbf{q}|\right)^{\sigma} \mathbf{q}\cdot(\mathbf{k}_1-\mathbf{q}) \\
\times \left(\frac{\mathbf{k}_1}{2}+\mathbf{k}_2\right)\cdot\left(\mathbf{q}-\frac{\mathbf{k}_1}{2}-\mathbf{k}_2\right) \\
\times \left(\frac{\mathbf{k}_1}{2}-\mathbf{k}_2\right)\cdot\left(\frac{\mathbf{k}_1}{2}+\mathbf{k}_2-\mathbf{q}\right) G_0(\hat{q}) G_0(\hat{k}_1-\hat{q}) \\
\times G_0\left(\hat{q}-\frac{\hat{k}_1}{2}-\hat{k}_2\right) G_0\left(\frac{\hat{k}_1}{2}+\hat{k}_2-\hat{q}\right), \qquad (21)
\end{aligned}
$$

where we have used a shorthand notation, e.g., $G(\hat{k}_1-\hat{q}) \equiv G(\mathbf{k}_1-\mathbf{q},\omega_1-\Omega)$. Using the change of variables $\mathbf{j}=\mathbf{q}-\mathbf{k}_1/2$, we get

$$
\begin{aligned}
\left(q\,|\mathbf{k}_1-\mathbf{q}|\right)^{\sigma}\mathbf{q}\cdot(\mathbf{k}_1-\mathbf{q}) \left(\frac{\mathbf{k}_1}{2}+\mathbf{k}_2\right)\cdot\left(\mathbf{q}-\frac{\mathbf{k}_1}{2}-\mathbf{k}_2\right)\left(\frac{\mathbf{k}_1}{2}-\mathbf{k}_2\right)\cdot\left(\frac{\mathbf{k}_1}{2}+\mathbf{k}_2-\mathbf{q}\right) \\
= j^{2\sigma+4}\left(\tfrac{1}{4}\cos^2(\theta_1)\; k_1^2 - k_2^2\cos^2(\theta_2)\right) + \mathrm{O}(k_i^2 k_j), \qquad (22)
\end{aligned}
$$

where $\mathbf{k}_i\cdot\mathbf{j} \equiv kj\cos\theta_i$. The contribution due to the bare propagator is a little involved, but we need to retain only the zeroth order contribution in k_i of the perturbative expansion, which greatly simplifies the calculation. Thus,

$$
\begin{aligned}
\lim_{\omega_1,\omega_2\to 0} G_0\left(\hat{j}+\frac{\hat{k}_1}{2}\right) G_0\left(\frac{\hat{k}_1}{2}-\hat{j}\right) G_0\left(\hat{j}-\hat{k}_2\right) G_0\left(\hat{k}_2-\hat{j}\right) \\
= \left[\left(\sum_{i=1}^{n} c_i j^{r_i}\right)^2 + \mathrm{O}(k_1) + \Omega^2\right]^{-1} \left[\left(\sum_{i=1}^{n} c_i j^{r_i}\right)^2 + \mathrm{O}(k_2) + \Omega^2\right]^{-1} \\
= (c_n j^{r_n})^{-4} (\hat{\Delta}_j^2 + \hat{z}^2)^{-2}, \qquad (23)
\end{aligned}
$$

where

$$
\hat{z} = \frac{\Omega}{c_n j^{r_n}}, \qquad \hat{\Delta}_j = 1 + \sum_{i=1}^{n-1} \frac{c_i}{c_n} j^{r_i - r_n} = -\frac{\sigma_j}{c_n j^{r_n}}. \qquad (24)
$$

J. Stat. Mech. (2011) P10030

The function $\hat{\Delta}_j$ evaluated at $j = \Lambda$ takes a positive value $\hat{\Delta}_\Lambda$ due to the signs of c_n and σ_Λ ($c_n > 0$ and $\sigma_\Lambda < 0$, see above and section 4). Hence, after integration in $\hat{z}$,

$$\int_{-\infty}^{+\infty} \mathrm{d}\hat{z} \left(\hat{\Delta}_j^2 + \hat{z}^2\right)^{-2} = \frac{\pi}{2\hat{\Delta}_j^3}, \tag{25}$$

this contribution reduces to

$$\begin{aligned}
\Gamma_1(\mathbf{k}_1, \mathbf{k}_2, 0, 0) &= \frac{2\lambda^2\Pi_0}{((k_1^2/4) - k_2^2)} \int_> \frac{\mathrm{d}\mathbf{j}}{(2\pi)^d} \frac{j^{2\sigma+4}}{4\hat{\Delta}_j^3 (c_n j^{r_n})^3} \left(\frac{1}{4}\cos^2(\theta_1)\; k_1^2 - k_2^2 \cos^2(\theta_2)\right) \\
&= \frac{\lambda^2\Pi_0 S_{d-1}}{2((k_1^2/4) - k_2^2)} \int_> \frac{\mathrm{d}j}{(2\pi)^d} \frac{j^{d+2\sigma+3}}{\hat{\Delta}_j^3 (c_n j^{r_n})^3} \\
&\quad \times \int_0^\pi \mathrm{d}\theta\, \sin^{d-2}(\theta) \left(\tfrac{1}{4}\cos^2(\theta)\, k_1^2 - k_2^2 \cos^2(\theta)\right) \\
&= \frac{\lambda^2\Pi_0}{2d} K_d \int_> \mathrm{d}j\, \frac{j^{d+2\sigma+3}}{(c_n j^{r_n})^3}\, \hat{\Delta}_j^{-3},
\end{aligned} \tag{26}$$

where $K_d = 2/[(4\pi)^{d/2}\Gamma(d/2)]$ is the surface area of the d-dimensional unit sphere S_d divided by $(2\pi)^d$, as defined in (A.8). We stop the calculation at this point because the remaining contributions to the vertex renormalization in (20) will be seen to cancel (26) exactly. Indeed, the function Γ_2 is given by the sum of the terms obtained from the noise contraction of $\mathbf{k}_1 - \mathbf{q}$ with $\mathbf{q} - \mathbf{k}_1$, i.e.,

$$\begin{aligned}
\Gamma_2(\mathbf{k}_1, \mathbf{k}_2, \omega_1, \omega_2) &= \frac{2\lambda^2\Pi_0}{((k_1^2/4) - k_2^2)} \int_> \frac{\mathrm{d}\mathbf{q}}{(2\pi)^d} \int \frac{\mathrm{d}\Omega}{2\pi} \left(q \left|\mathbf{q} - \frac{\mathbf{k}_1}{2} - \mathbf{k}_2\right|\right)^\sigma \\
&\quad \times \mathbf{q}\cdot(\mathbf{k}_1 - \mathbf{q}) \left(\frac{\mathbf{k}_1}{2} + \mathbf{k}_2\right) \cdot \left(\mathbf{q} - \frac{\mathbf{k}_1}{2} - \mathbf{k}_2\right) \left(\frac{\mathbf{k}_1}{2} - \mathbf{k}_2\right) \cdot (\mathbf{q} - \mathbf{k}_1) \\
&\quad \times G_0(\hat{q}) G_0(\hat{k}_1 - \hat{q}) G_0(\hat{q} - \hat{k}_1) G_0\left(\hat{q} - \frac{\hat{k}_1}{2} - \hat{k}_2\right),
\end{aligned} \tag{27}$$

where

$$\begin{aligned}
&\left(q \left|\mathbf{q} - \frac{\mathbf{k}_1}{2} - \mathbf{k}_2\right|\right)^\sigma \mathbf{q}\cdot(\mathbf{k}_1 - \mathbf{q}) \left(\frac{\mathbf{k}_1}{2} + \mathbf{k}_2\right) \cdot \left(\mathbf{q} - \frac{\mathbf{k}_1}{2} - \mathbf{k}_2\right) \left(\frac{\mathbf{k}_1}{2} - \mathbf{k}_2\right) \cdot (\mathbf{q} - \mathbf{k}_1) \\
&\qquad = -j^{2\sigma+4} \left(\tfrac{1}{4}\cos^2(\theta_1)\, k_1^2 - k_2^2 \cos^2(\theta_2)\right) + \mathrm{O}(k_i^2 k_j)
\end{aligned} \tag{28}$$

and

$$\begin{aligned}
&\lim_{\omega_1,\omega_2 \to 0} G_0\left(\hat{j} + \frac{\hat{k}_1}{2}\right) G_0\left(\frac{\hat{k}_1}{2} - \hat{j}\right) G_0\left(\hat{j} - \frac{\hat{k}_1}{2}\right) G_0(\hat{j} - \hat{k}_2) \\
&\qquad = (c_n j^{r_n})^{-4} \left[(\hat{\Delta}_j^2 + \hat{z}^2)(\hat{\Delta}_j - \mathrm{i}\hat{z})^2\right]^{-1}.
\end{aligned} \tag{29}$$

Following similar steps to the case of Γ_1, after integration in $\hat{z}$,

$$\int_{-\infty}^{+\infty} \mathrm{d}\hat{z} \left[(\hat{\Delta}_j^2 + \hat{z}^2)(\hat{\Delta}_j \pm \mathrm{i}\hat{z})^2\right]^{-1} = \frac{\pi}{4\hat{\Delta}_j^3}, \tag{30}$$

J. Stat. Mech. (2011) P10030

we get

$$\Gamma_2(\mathbf{k}_1,\mathbf{k}_2,0,0) = -\frac{\lambda^2\Pi_0}{4d}K_d\int_> \mathrm{d}j\,\frac{j^{d+2\sigma+3}}{(c_n j^{r_n})^3}\,\hat{\Delta}_j^{-3}. \tag{31}$$

Finally, the contribution Γ_3 in (20) arises from a contraction of noise components with wavevectors $\mathbf{q}$ and $-\mathbf{q}$. This contribution reads

$$\begin{aligned}\Gamma_3(\mathbf{k}_1,\mathbf{k}_2,\omega_1,\omega_2) = {} & \frac{2\lambda^2\Pi_0}{((k_1^2/4)-k_2^2)}\int_> \frac{\mathrm{d}\mathbf{q}}{(2\pi)^d}\int\frac{\mathrm{d}\Omega}{2\pi}\left(|\mathbf{k}_1-\mathbf{q}|\left|\frac{\mathbf{k}_1}{2}+\mathbf{k}_2-\mathbf{q}\right|\right)^{\sigma}\\ & \times\,\mathbf{q}\cdot(\mathbf{k}_1-\mathbf{q})\,(-\mathbf{q})\cdot\left(\frac{\mathbf{k}_1}{2}+\mathbf{k}_2\right)\left(\frac{\mathbf{k}_1}{2}-\mathbf{k}_2\right)\cdot\left(\frac{\mathbf{k}_1}{2}+\mathbf{k}_2-\mathbf{q}\right)\\ & \times\,G_0(\hat{q})G_0\,(-\hat{q})\,G_0\left(\hat{k}_1-\hat{q}\right)G_0\left(\frac{\hat{k}_1}{2}+\hat{k}_2-\hat{q}\right),\end{aligned} \tag{32}$$

where

$$\begin{aligned}&\left(|\mathbf{k}_1-\mathbf{q}|\left|\frac{\mathbf{k}_1}{2}+\mathbf{k}_2-\mathbf{q}\right|\right)^{\sigma}\mathbf{q}\cdot(\mathbf{k}_1-\mathbf{q})\,(-\mathbf{q})\cdot\left(\frac{\mathbf{k}_1}{2}+\mathbf{k}_2\right)\left(\frac{\mathbf{k}_1}{2}-\mathbf{k}_2\right)\cdot\left(\frac{\mathbf{k}_1}{2}+\mathbf{k}_2-\mathbf{q}\right)\\ &\quad = -j^{2\sigma+4}\left(\tfrac{1}{4}\cos^2(\theta_1)\,k_1^2-k_2^2\cos^2(\theta_2)\right)+\mathrm{O}(k_i^2k_j),\end{aligned} \tag{33}$$

and

$$\begin{aligned}&\lim_{\omega_1,\omega_2\to 0}G_0\left(\hat{j}+\frac{\hat{k}_1}{2}\right)G_0\left(-\hat{j}-\frac{\hat{k}_1}{2}\right)G_0\left(\hat{j}-\frac{\hat{k}_1}{2}\right)G_0(\hat{j}-\hat{k}_2)\\ &\quad = (c_nj^{r_n})^{-4}\,[(\hat{\Delta}_j^2+\hat{z}^2)(\hat{\Delta}_j+\mathrm{i}\hat{z})^2]^{-1}.\end{aligned} \tag{34}$$

Thus, in parallel with the previous cases, in the $\omega_{1,2}\to 0$ limit we obtain $\Gamma_3=\Gamma_2=-\Gamma_1/2$. Hence from equation (20) finally $\lambda^<=\lambda$, so that the nonlinear term does not renormalize at one loop order. Note, this result does not make any requirement on the morphological stability of the system described by equation (19), and has the analogous vertex cancellations for both the KPZ and the Lai–Das Sarma–Villain (LDV) equations as immediate corollaries. As is well known, for the former this property leads to the scaling relation $\alpha+z=2$ at the nonlinear fixed point, and is usually associated with the explicit invariance of the equation under a Galilean transformation [1, 2, 26]. However, for the LDV equation an analogous symmetry is known *not to* exist [56]. This fact makes it appear as a coincidence that the KPZ equation does combine such a type of (Galilean) symmetry *with* vertex cancellation. Admittedly, vertex cancellation also occurs at two loop order in the KPZ equation [57, 58], but not in the LDV case [56], so that the interplay between Galilean symmetry and the so-called Galilean scaling relation is subtle. Still, more recent works also question a causal relation between the two. Thus, it has been argued that for the Navier–Stokes (NS) and related equations, such as Burgers' equation, Galilean invariance does not enforce vertex non-renormalization [59]. These arguments have been further substantiated more recently [60, 61] within a field-theoretical approach to the stochastic NS system. Likewise, recently models or discretization schemes of the KPZ equation have been shown to explicitly break Galilean invariance while fulfilling the $\alpha+z=2$ scaling relation, see [62, 63] and references therein.

J. Stat. Mech. (2011) P10030

4. Dynamic renormalization group flow and fixed points

Coming back to equation (4), in order to account for its scaling properties, we restrict our DRG analysis to the case $m = 2$ and $\mathcal{N} = 0$, that is,

$$\partial_t h_{\mathbf{k}}(t) = (-\nu k^{\mu} - \mathcal{K}k^2)h_{\mathbf{k}}(t) + \frac{\lambda}{2}\mathcal{F}[(\nabla h)^2]_{\mathbf{k}} + \eta_{\mathbf{k}}(t). \tag{35}$$

For clarity of the exposition, the details of the corresponding DRG calculations are left to appendix A. Actually, the scaling properties of the equation do not change when we take into account a dispersion relation with additional stabilizing relaxation terms, less relevant than k^2, namely, $n > 2$ in equation (4). A proof of this is given in appendix B for the specific $\mu = 1$ case, considering $\mathcal{N} \neq 0$, with $n = 3$, and 4.

After coarse-graining of propagator and noise variance (as in appendix A), and the vertex (as in section 3.1), the final step in the DRG method is the application of a rescaling that restores the initial value of the wavevector cut-off. Moreover, this allows us to write parameter renormalization in a differential form, taking l as the independent variable. We can actually employ the formulas (7), where the role of unscaled parameters is now taken by our coarse-grained estimates $\nu^<$, etc and scaled quantities $\tilde{\nu}$, etc become finally the renormalized parameters. This makes explicit the non-trivial effect of the coarsening step as, e.g., $\nu^<$ differs from the bare parameter ν in the original equation. After taking the $\delta l \to 0$ limit, the ensuing infinitesimal parameter variation constitutes the one loop RG flow for arbitrary substrate dimension d (see appendix A),

$$\frac{\mathrm{d}\nu}{\mathrm{d}l} = \nu\,[z - \mu]\,, \qquad \frac{\mathrm{d}\lambda}{\mathrm{d}l} = \lambda\,[\alpha + z - 2]\,, \tag{36}$$

$$\frac{\mathrm{d}\mathcal{K}}{\mathrm{d}l} = \mathcal{K}\left[z - 2 - \frac{\lambda^2\Pi_0 K_d}{4d}\,\frac{(d-2)\mathcal{K} + (d-\mu)\nu}{\mathcal{K}\,(\mathcal{K}+\nu)^3}\right], \tag{37}$$

$$\frac{\mathrm{d}\Pi_0}{\mathrm{d}l} = \Pi_0\left[z - 2\alpha - d + \frac{\lambda^2\Pi_0 K_d}{4\,(\mathcal{K}+\nu)^3}\right]. \tag{38}$$

Without loss of generality, in equations (36)–(38) we have fixed the lattice cut-off, $\Lambda = 1$, bearing in mind that in order to avoid the finite pole of the bare propagator, the coarse-graining step has been performed in an infinitesimal shell $k \in [\Lambda(1 - \delta l), \Lambda]$ within the band of linearly stable (large) wavevector values [20]. The dispersion relation for $k = \Lambda$ (the largest wavenumber) can be written as

$$\sigma_\Lambda = -\mathcal{K}\Lambda^2\left(1 + \frac{\nu}{\mathcal{K}}\Lambda^{\mu-2}\right) = -\mathcal{K}\Lambda^2\Delta_\Lambda, \tag{39}$$

where $\Delta_k = 1 + \nu\mathcal{K}^{-1}|k|^{\mu-2}$ is employed in the evaluation of the integrals in equations (13) and (17). The sign of σ_Λ gives us a criterion to identify a physically consistent DRG flow (see appendix A for details). Note that σ_Λ has to be negative in order to have a well-behaved dispersion relation and that, for the same reason, $\mathcal{K}$ has to be positive. Thus, equation (39) implies that Δ_Λ has to be a positive quantity. All the fixed points obtained within the DRG approach have to satisfy this requirement.

Equations (36)–(38) generalize the KPZ flow in a natural way for non-zero ν, and inherit the known analytical limitations of the latter [1, 2, 26]. Still, they carry valuable

J. Stat. Mech. (2011) P10030

information. Introducing the following coupling parameters [44]

$$g = \frac{\lambda^2 \Pi_0 K_d}{4(\mathcal{K}+\nu)^3}, \qquad f = \frac{\mathcal{K}}{\mathcal{K}+\nu}, \tag{40}$$

we can calculate their flow using equations (36)–(38). Thus,

$$\frac{\mathrm{d}f}{\mathrm{d}l} = (1-f)\left\{(\mu-2)f - \frac{g}{d}\left[(d-2)f + (d-\mu)(1-f)\right]\right\}, \tag{41}$$

$$\frac{\mathrm{d}g}{\mathrm{d}l} = g\left\{6f - 4 - d + g + 3\mu(1-f) + 3\,\frac{g}{d}[(d-2)f + (d-\mu)(1-f)]\right\}. \tag{42}$$

The ratio between the (possibly) morphologically destabilizing parameter, ν, and the stabilizing one, $\mathcal{K}$, follows from the exact relation $1-f = \nu/(\nu+\mathcal{K})$. The condition $\Delta_\Lambda \geq 0$ is satisfied as long as these two couplings are positive or zero; for this reason we can restrict the DRG flow analysis to the first quadrant of the (f,g) plane. Then, a bare parameter choice corresponding to the morphologically unstable condition $\nu(l=0) < 0$ implies $f(l=0) > 1$, while the converse condition $f(l=0) < 1$ corresponds to morphological stability in terms of the bare parameters. The line $f = 1$ (at which $\nu = 0$) is actually never crossed by any trajectory, since flow lines cannot cross each other in this autonomous flow and $f = 1$ is clearly invariant under the iteration. Note, $f = 1$ implies $\nu = 0$, so that no explicit renormalization of ν from negative to positive values is allowed by the flow (41)–(42). Thus, dynamical stabilization of the early-time morphological instability for equation (35), and thus for equation (4), cannot take place through Yakhot's mechanism (namely, 'surface tension' renormalization) for the Kuramoto–Sivashinsky equation [24]. This agrees, moreover, with expectations based on a naive power counting analysis of both equations that would lead *not* to expect RG corrections to a k^μ term from a k^2 term that is irrelevant in comparison for $\mu < 2$.

The fixed points of the RG flow are given by the values of the pair (f,g) for which equations $\mathrm{d}f/\mathrm{d}l = 0$ and $\mathrm{d}g/\mathrm{d}l = 0$ hold simultaneously. Obviously, $f = 1$ and $g = 0$ satisfy the first and the second equations, respectively. Moreover, the rhs of equation (41) is identically zero for

$$f = \frac{g(d-\mu)}{(\mu-2)(d-g)}, \tag{43}$$

while relation

$$g = \frac{3\mu(f-1) + 4 + d - 6f}{3\left[(d-2)f + (d-\mu)(1-f)\right]/d + 1}, \tag{44}$$

leads to $\mathrm{d}g/\mathrm{d}l = 0$.

A detailed analysis of equations (41)–(42) yields the same fixed point structure as for the KPZ equation [2]—namely, the Edwards–Wilkinson (EW) fixed points at $(f,g) = (1,0)$ and, for appropriate values of d (see section 5), the KPZ fixed point at $(f,g) = (1,1/2)$—, with the addition of two new non-trivial fixed points. One corresponds to the morphologically stable interfaces (we call it *Smooth* fixed point), being located at the origin of the (f,g) plane. Its dynamic exponent is $z = \mu$, while hyperscaling holds, namely, $z = 2\alpha + d$. Note that a zero value for g means that the nonlinear term λ is vanishing and (35) becomes a linear equation, the Smooth fixed point being the

doi:10.1088/1742-5468/2011/10/P10030

J. Stat. Mech. (2011) P10030

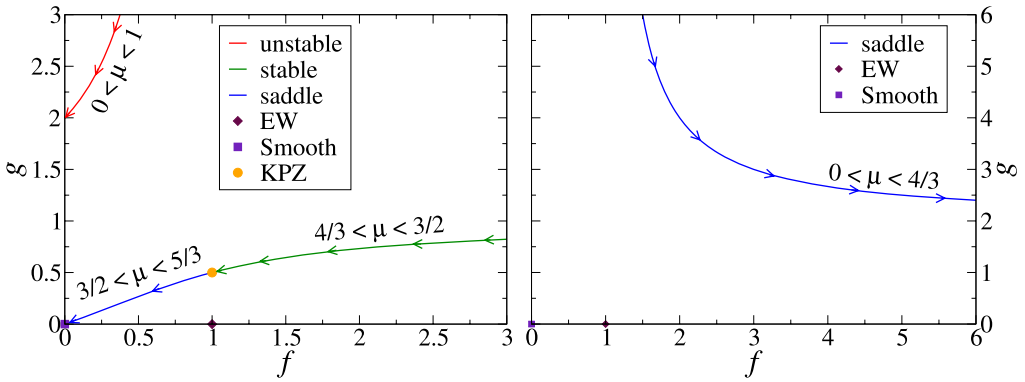

Figure 1. Position of the Galilean fixed point on the (f, g) plane for $d = 1$ (left panel) and $d = 2$ (right panel). Arrows and colors indicate, respectively, the displacement of this fixed point for increasing μ, and its stability. The intervals of μ specified near the solid lines provide the values of μ at which stability changes for this fixed point.

one employed in our discussion on the critical dimension in section 2. Actually, at the linear EW and Smooth fixed points, the equation becomes variational and hyperscaling ensues, relating the dynamic and roughness exponents. Hyperscaling is associated with non-renormalization of the noise amplitude [26] given that, under these conditions, the equation has (in the morphologically stable condition) the asymptotic height distributions $\mathcal{P}_{\rm EW}[h] \propto \exp[(-\mathcal{K}/(2\Pi_0)) \int k^2 |h_{\mathbf{k}}|^2 \, {\rm d}\mathbf{k}]$ or $\mathcal{P}_{\rm Smooth}[h] \propto \exp[(-\nu/(2\Pi_0)) \int k^\mu |h_{\mathbf{k}}|^2 \, {\rm d}\mathbf{k}]$ at the EW and Smooth fixed points, respectively.

The second new fixed point that exists for the flow (41)–(42) implements, as the KPZ fixed point, the scaling relation $\alpha + z = 2$ usually associated with Galilean invariance, and we thus we call it *Galilean* fixed point. It is the one found in simulations for the morphologically unstable condition with $\nu < 0$ [33]. As in the Smooth fixed point, the dynamic exponent takes the value expected from power counting, $z = \mu$. The coordinates of the Galilean fixed point, (f_*, g_*), are given by equating (43) to (44), namely,

$$f_* = \frac{g_*(d-\mu)}{(\mu-2)(d-g_*)}, \qquad g_* = d + 4 - 3\mu. \tag{45}$$

Besides, this fixed point has to satisfy the conditions $f_* \geq 0$ and $g_* \geq 0$, hence it is not defined for some values of μ in the $(0, 2]$ interval. Indeed, the condition $g_* \geq 0$ leads to an admissible value for this coupling for $\mu \leq (d + 4)/3$. For a fixed value of μ, this is equivalent to the $d > d_{\rm c}$ condition using the value of the critical dimension derived in section 2 for the morphologically stable case. The second condition, i.e. $f_* > 0$, has to be analyzed carefully. In fact, for $d < 4/3$, the Galilean fixed point occurs for μ within the intervals $(0, d] \bigcup (4/3, (d + 4)/3]$ (for $d = 1$, see the left panel of figure 1). In the case $4/3 \leq d < 2$, the admissibility intervals are $(0, 4/3) \bigcup [d, (d + 4)/3]$. Finally, for $d \geq 2$, we have only one condition for the existence of the Galilean fixed point, namely, $\mu < 4/3$, as illustrated on the right panel of figure 1.

In order to study the stability of these fixed points, we have to compute the derivatives of (41) and (42) with respect to the couplings, and evaluate the eigenvalues of the linear stability matrices. So far, we have outlined the main steps we have taken to obtain the

Table 1. Fixed points in $1+1$ growth dimensions ($d=1$). In the first column, G stands for Galilean and S for Smooth, according to the terminology introduced in the main text. In the last column, $\lambda_{1,2}$ are the eigenvalues of the linear stability matrix at the corresponding fixed point. Their real parts, $v_{1,2}^{(1)}$, are plotted in figure 2 in the case of the Galilean fixed point. The latter is not defined in the intervals $1<\mu\leq 4/3$ and $5/3<\mu\leq 2$.

Name	f	g	z	α	β	Scaling relation	λ_1	λ_2
EW	1	0	2	$1/2$	$1/4$	$2\alpha+d=z$	$2-\mu$	1
KPZ	1	$1/2$	$3/2$	$1/2$	$1/3$	$\alpha+z=2$	$3/2-\mu$	-1
S	0	0	μ	$\dfrac{\mu-1}{2}$	$\dfrac{\mu-1}{2\mu}$	$2\alpha+d=z$	$\mu-2$	$3\mu-5$
G	$\dfrac{(5-3\mu)(1-\mu)}{(\mu-2)(3\mu-4)}$	$5-3\mu$	μ	$2-\mu$	$\dfrac{2-\mu}{\mu}$	$\alpha+z=2$	$v_1^{(1)}$	$v_2^{(1)}$

fixed points of the DRG flow. In the next section we provide details on their stability for various substrate dimensions (in particular, $d=1$, $d=2$, and $d>2$).

5. Fixed point stability and dependence with dimension

The study of the trajectories of the RG flow provides useful information on the stability of the different fixed points. Although the stable case has been already examined in the context of the fractal KPZ (FKPZ) equation [31] (which is obtained from (4) when $\nu>0$ and $\mathcal{K}=\mathcal{N}=0$), our DRG study supplies additional information. In [31] the FKPZ equation was studied by means of a self-consistent expansion (SCE) for spatially correlated noise in the case of arbitrary substrate dimension. The limit of Gaussian white noise is recovered when the exponent of the noise correlations introduced in [31] is equal to zero. Although the SCE allows the identification of the strong coupling KPZ fixed point with a reasonable accuracy ($\alpha=0.295$ and $z=1.705$ for $d=2$, compatible with the most reliable estimates for this value of d [64]), the SCE method has some drawbacks. Even though all the fixed points reported in section 4 appear within the SCE analysis, this method cannot assess which fixed point is selected by the dynamics during the growth process. For example, in the case of $d=2$, three different phases are found [31], each one with different values for the critical exponents. For some value of the exponent of the fractional Laplacian (μ in our notation, that is equivalent to $2-\rho$ in [31]), all these phases are admissible, there being no analytical criterion for the selection of one of them. The present section is precisely devoted to the analysis of the DRG predictions on the fixed point that is selected asymptotically by the dynamics for each substrate dimension, and as a function of bare parameter values.

5.1. One-dimensional interfaces

For $d=1$ we obtain three fixed points whose coordinates do not depend on the exponent μ, i.e., the Smooth, EW, and KPZ fixed points (see left panel of figure 1). On the contrary, the Galilean fixed point changes location in the (f,g) plane by changing the value of μ.

J. Stat. Mech. (2011) P10030

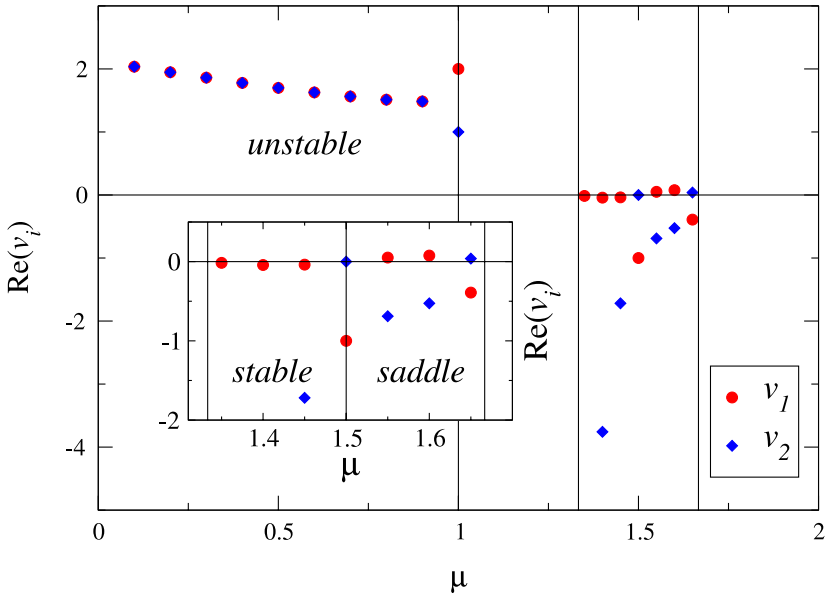

Figure 2. Real parts of the eigenvalues of the linear stability matrix of the Galilean fixed point for $d = 1$, as functions of μ. The inset is a zoom of the region $4/3 < \mu < 5/3$ within which the fixed point changes stability from stable to saddle at $\mu = 3/2$.

In table 1 we summarize all the fixed points that exist for $d = 1$, their critical exponents, and the eigenvalues of their stability matrix. The (real parts of the) two eigenvalues of the Galilean fixed point, $v_{1,2}^{(1)}$, have been obtained numerically; we show in figure 2 how they change as functions of μ.

In figure 3 we show eight representative snapshots of the RG flow for $d = 1$. For $0 < \mu \leq 1$, the Galilean fixed point is unstable and moves on the sector of the (f, g) plane associated with morphologically stable bare conditions $f < 1$, following the red line in the left panel of figure 1. Qualitatively, within this interval of μ, the flow behaves as in figures 3(a)–(c), in which the DRG flow is shown for the cases $\mu = 1/4, 1/2, 1$. Notice that the only finite fixed point for $f < 1$ and $0 < \mu < 4/3$ is the Smooth fixed point, as expected from power counting. For $\mu \in (1, 4/3]$, the Galilean fixed point is not an admissible solution of the DRG flow equations (41) and (42), and it disappears (for example, see figure 3(d)) until μ becomes larger than $4/3$, when it reenters the phase portrait as a fixed point for morphologically unstable bare conditions $f > 1$, see e.g. figure 3(e). Meanwhile, the basin of attraction of the Smooth fixed point changes as a function of μ, see figures 3(a)–(c).

For larger μ values in the interval $4/3 < \mu \leq 3/2$, the Galilean fixed point becomes stable, attracting all the trajectories with $f > 1$; this condition is shown in figure 3(e). The remaining trajectories are attracted by the Smooth fixed point. Actually, the Galilean fixed point merges with the KPZ fixed point at exactly $\mu = z_{\rm KPZ}(d = 1) = 3/2$ (see left panel of figure 1 and figure 3(f)), losing stability in favor of the latter for larger values, $z_{\rm KPZ}(1) \leq \mu \leq 2$, justifying the observation of KPZ scaling in this range of μ, as obtained in numerical simulations under morphologically unstable parameter choices [33].

J. Stat. Mech. (2011) P10030

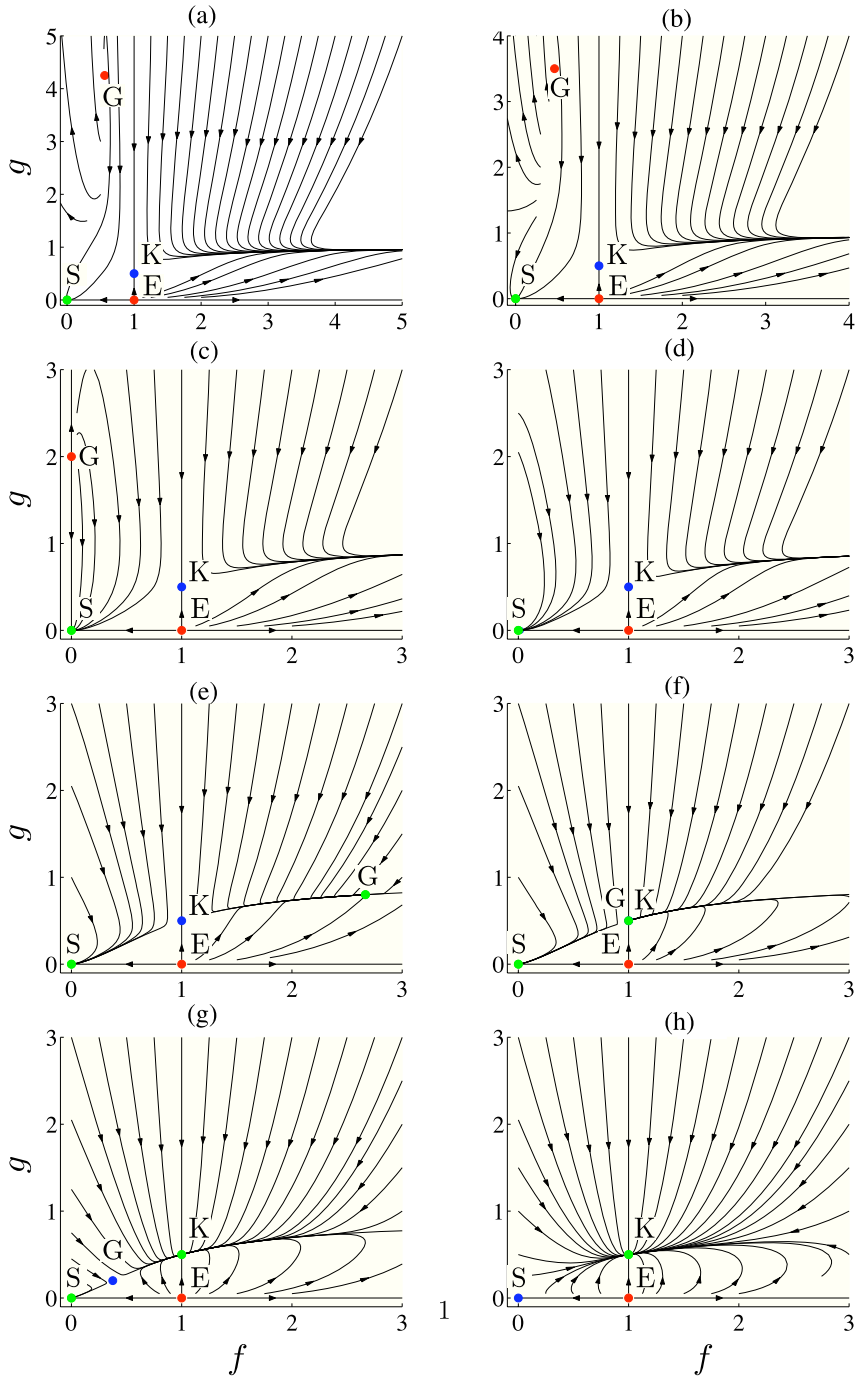

Figure 3. Numerical integration of equations (41)–(42) for $d = 1$ and different values of the exponent μ: (a) $\mu = 1/4$, (b) $\mu = 1/2$, (c) $\mu = 1$, (d) $\mu = 1.15$, (e) $\mu = 1.4$, (f) $\mu = 3/2$, (g) $\mu = 1.6$, (h) $\mu = 1.8$. The values of the coupling variables at the different fixed points (in the graphs, E stands for Edwards–Wilkinson, K for KPZ, S for Smooth, and G for Galilean) and the associated critical exponents are reported in table 1. The color of each fixed point represents its stability (red stands for unstable, blue for saddle, and green for stable). Note that the Galilean fixed point changes with μ, merging with the KPZ fixed point at $\mu = 3/2$.

J. Stat. Mech. (2011) P10030

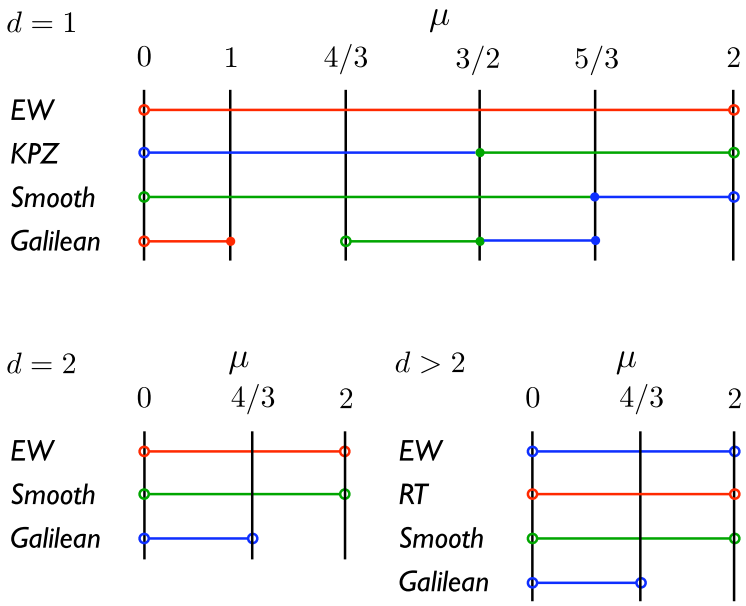

Figure 4. Stability of the fixed points for $d = 1, 2$ and $d > 2$. As before the red stands for unstable, blue for saddle and green for stable fixed point.

For $3/2 < \mu \leq 5/3$, the Galilean fixed point becomes a saddle, being located on the separatrix between the basins of attraction of the two stable fixed points for the DRG flow, the Smooth and the KPZ fixed points, see figure 3(g), back on the morphologically stable sector. For $\mu > 5/3$, the Galilean fixed point is no longer an admissible solution of the RG equations, and disappears. The only stable fixed point for these values of μ is the KPZ fixed point (see figure 3(h)). As mentioned above, indeed it is KPZ scaling that is obtained in numerical simulations [33] performed for this range of μ values for morphologically unstable conditions. Actually, preliminary simulations performed for stable parameter conditions seem to agree with this conclusion also [65], which in turn was expected from the power counting analysis performed in section 2 above. In the first row of figure 4 we summarize the DRG stability of the four fixed points as a function of μ. Note, numerical simulations for the morphologically unstable condition predict scaling as for the Galilean fixed point when $0 < \mu < 4/3$ [33], and thus do not agree with the DRG flow, probably due to the assumptions made in the perturbative expansion. Nevertheless, the DRG analysis gives significant hints about the critical behavior of this non-local class of growth equations, in particular the change of universality class from that associated with the Galilean fixed point for $0 < \mu < z_{\rm KPZ}(d = 1)$ to KPZ scaling for $z_{\rm KPZ}(d = 1) < \mu \leq 2$, generalizing, in particular, known results for the noisy Kuramoto–Sivashinsky equation [20, 21], that is, the $\mu = 2$ case of equation (4).

5.2. Two-dimensional interfaces

The situation changes drastically for $d = 2$. As expected for perturbative approaches such as DRG [27] and even field-theoretical schemes [57, 58], there is no finite KPZ fixed point for the RG flow, while the Galilean fixed point remains finite only up to $\mu = 4/3 < z_{\rm KPZ}(2) \simeq 1.61$. For $\mu = 4/3$, this fixed point is at $f = \infty$ and $g = 2$, see

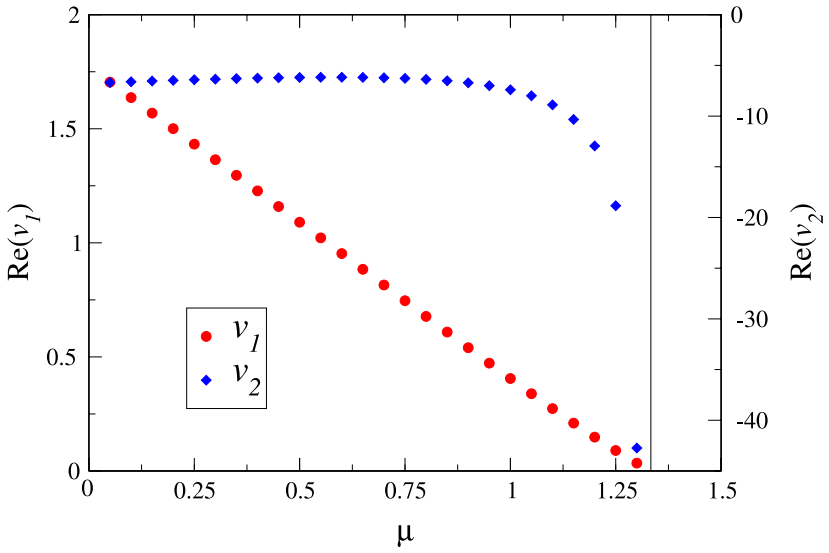

Figure 5. Real parts of the eigenvalues of the linear stability matrix for the Galilean fixed point for $d = 2$, as functions of μ. Note the different scales used on the left (for $\mathrm{Re}(v_1)$) and the right (for $\mathrm{Re}(v_2)$) vertical axes of the graph.

Table 2. Finite fixed points in $2 + 1$ growth dimensions ($d = 2$). The meaning of G, S, $\lambda_{1,2}$, and $v_i^{(2)}$ is as in table 1. The real parts, $v_{1,2}^{(2)}$, of the eigenvalues of the Galilean fixed point are plotted in figure 5. This fixed point is not defined for $\mu \geq 4/3$.

Name	f	g	z	α	β	Scaling relation	λ_1	λ_2
EW	1	0	2	0	0	$2\alpha + d = z$	$2 - \mu$	0
S	0	0	μ	$\frac{\mu-2}{2}$	$\frac{\mu-2}{2\mu}$	$2\alpha + d = z$	$\mu - 2$	$3(\mu - 2)$
G	$\frac{3(\mu-2)}{3\mu-4}$	$3(2-\mu)$	μ	$2 - \mu$	$\frac{2-\mu}{\mu}$	$\alpha + z = 2$	$v_1^{(2)}$	$v_2^{(2)}$

the right panel of figure 1. As in the $d = 1$ case, the position of the Galilean fixed point depends on the value of μ, as shown in the right panel of figure 1. In table 2 we summarize the results for the fixed points in the two-dimensional case, showing in figure 5 the real parts of the eigenvalues of the Galilean fixed point, $v_{1,2}^{(2)}$, as functions of μ. We observe that the stability of the three fixed points does not change with μ (see the second row of figure 4).

We can identify two main features in this DRG flow. The first one is represented in figures 6(a)–(c). In this case the Galilean fixed point influences all trajectories in the morphologically unstable region $f > 1$; in fact, it is located on the manifold that separates two classes of trajectories: asymptotically, one type of trajectory flows toward $f = 1$ and $g \to \infty$; the other type of trajectory flows toward $f \to \infty$ and $g = 2$, see figures 6(a)–(c). Within the morphologically stable region $f < 1$, the Smooth fixed point attracts some trajectories, while those outside the basin of attraction of this fixed point flow asymptotically to $f = 0$ and $g \to \infty$.

J. Stat. Mech. (2011) P10030

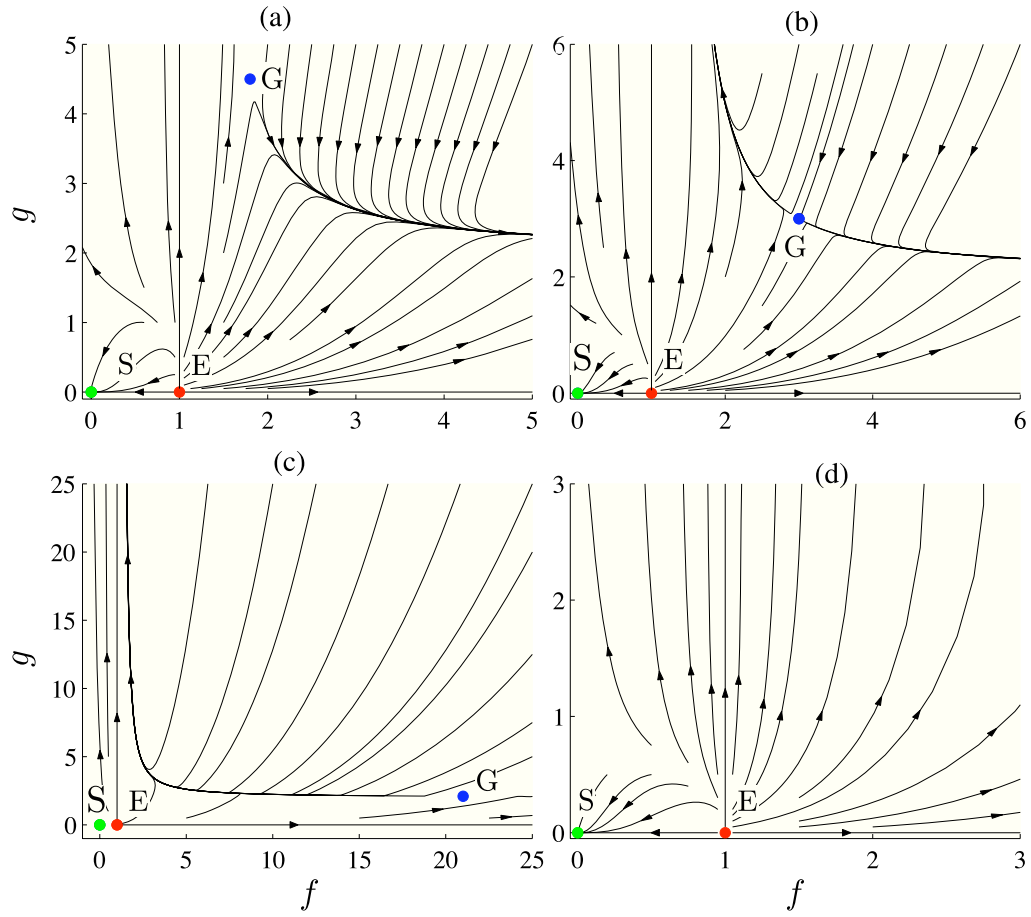

Figure 6. Numerical integration of equations (41)–(42) for $d = 2$ and different values of the exponent μ: (a) $\mu = 1/2$, (b) $\mu = 1$, (c) $\mu = 1.3$, (d) $\mu = 3/2$. The values of the coupling variables at the different fixed points (in the graphs, E stands for Edwards–Wilkinson, K for KPZ, S for Smooth and G for Galilean) and the associated critical exponents are reported in table 2. The color of each fixed point represent its stability (red stands for unstable, blue for saddle and green for stable). Note that the Galilean fixed point is not present for $\mu \geq 3/4$.

For $\mu \geq 4/3$, the Galilean fixed point is not an admissible solution of the flow equations. In this case all trajectories with $f > 1$ flow to $f \to 1$ and $g \to \infty$, attracted by the KPZ fixed point at infinity, see figure 6(d). The region with $f < 1$ does not display any qualitative change as compared to the case $\mu < 4/3$. To compare with the present results of the DRG analysis, numerical simulations of the morphologically unstable case of equation (4) [33] for $d = 2$ indicate Galilean scaling for $\mu < z_{\rm KPZ}(2) \simeq 1.61$ and KPZ scaling for $z_{\rm KPZ}(2) < \mu \leq 2$.

5.3. The general case $d > 2$

For d larger than two, we obtain a flow behavior that is independent of the substrate dimension. As for the KPZ case, there is no finite fixed point associated with KPZ scaling, while we do find an unstable fixed point located at $f = 1$ (i.e., $\nu = 0$) and $g = g_{\rm RT}(d)$

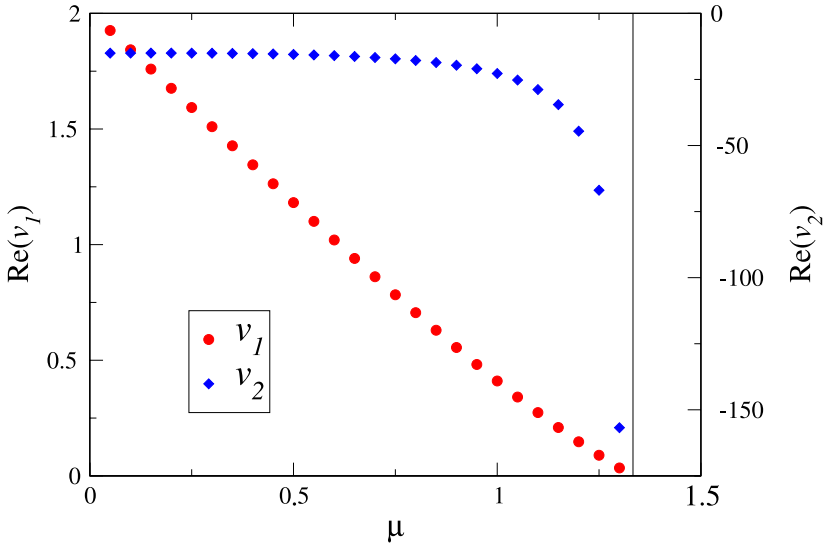

Figure 7. Real parts of the eigenvalues of the linear stability matrix $S(\mathrm{G})$ for the Galilean fixed point for $d = 3$, as functions of μ. Note the different scales used on the left (for v_1) and the right (for v_2) vertical axes of the graph.

Table 3. Fixed points in $d+1$ growth dimensions for $d > 2$. The meaning of G, S, $\lambda_{1,2}$, and $v_{1,2}^{(d)}$ is as in tables 1 and 2. RT denotes the fixed point controlling the roughening transition, as discussed in the main text. The coordinates of the Galilean fixed point depend on d as given by equations (45). This fixed point is not defined for $\mu = 3/2$.

Name	f	g	z	α	β	Scaling relation	λ_1	λ_2
EW	1	0	2	$(2-d)/2$	$(2-d)/4$	$2\alpha + d = z$	$2-\mu$	$2-d$
RT	1	$\dfrac{d(d-2)}{4d-6}$	$2+\dfrac{(d-2)^2}{4d-6}$	$\dfrac{(d-2)^2}{6-4d}$	$\dfrac{(d-2)^2}{8-4d-d^2}$	$\alpha + z = 2$	$2-\mu+\dfrac{(d-2)^2}{4d-6}$	$d-2$
S	0	0	μ	$\dfrac{\mu-d}{2}$	$\dfrac{\mu-d}{2\mu}$	$2\alpha + d = z$	$\mu-2$	$3\mu-d-4$
G	f_*	g_*	μ	$2-\mu$	$\dfrac{2-\mu}{\mu}$	$\alpha + z = 2$	$v_1^{(d)}$	$v_2^{(d)}$

that is associated with the non-equilibrium *roughening transition* (RT) [1], hence our terminology. Starting from a bare parameter condition corresponding to $f(0) = 1$, the parameters of equation (4) flow toward the EW fixed point for $g(0) < g_{\mathrm{RT}}$, or toward the strong coupling regime associated with KPZ scaling for $g(0) > g_{\mathrm{RT}}$. See table 3 for the value of g_{RT} as a function of d. For this reason, the EW fixed point acquires a stable direction as compared with smaller values of d, changing from unstable (for $d = 2$) to saddle type. The two other fixed points, Smooth and Galilean, have the same stability and exponents as found for $d = 2$ (take into account that a negative roughening exponent means subleading corrections to scaling). We summarize the results for $d > 2$ in table 3.

J. Stat. Mech. (2011) P10030

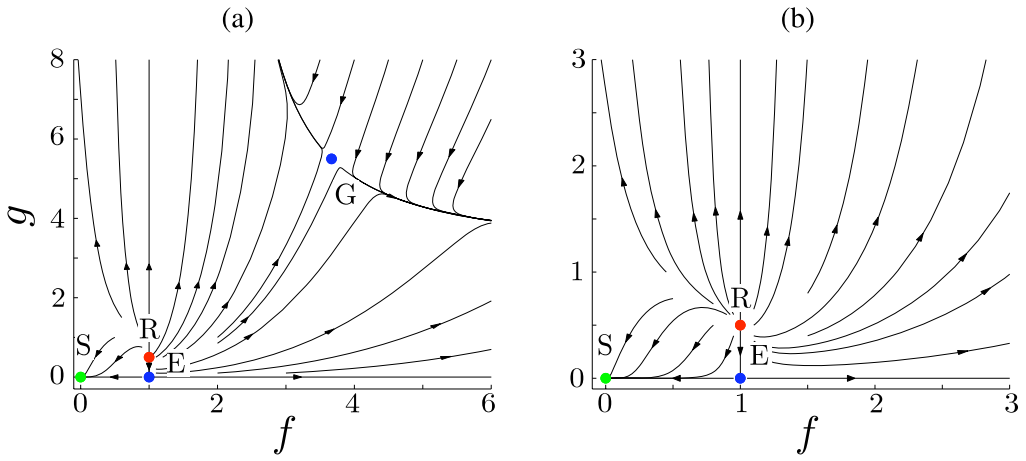

Figure 8. Numerical integration of equations (41)–(42) for $d = 3$ and different values of the exponent μ: (a) $\mu = 1/2$, (b) $\mu = 3/2$. The values of the coupling variables at the different fixed points (in the graphs, E stands for Edwards–Wilkinson, R for the fixed point related to the roughening transition, S for Smooth and G for Galilean) and the associated critical exponents are reported in table 3. The color of each fixed point represent its stability (red stands for unstable, blue for saddle and green for stable). Note that the Galilean fixed point is not present for $\mu = 3/2$.

As seen in the last two columns of table 3, the signs of λ_1 and λ_2 do not depend on d, implying the independence of the stability of these four fixed points on the substrate dimensionality (note that, for the RT fixed point, $\lambda_1 > 0$ for every $0 < \mu \leq 2$). The real parts of the eigenvalues for the Galilean fixed point are plotted in figure 7 for $d = 3$. As in the case of two-dimensional interfaces, one eigenvalue is positive whereas the other one is negative. We have checked that this behavior is not changed by increasing the value of d.

Beyond fixed point stability, and similarly to the KPZ equation, for any $d > 2$ the structure of the RG flow is almost identical to the two-dimensional case, the only difference being that the $f = 1$ line acquires the RT fixed point, giving the possibility to observe EW scaling for $\nu = 0$. In figure 8 we report two representative flows for $d = 3$. By comparing them with those reported in figures 6(a) and (d), one cannot appreciate any qualitative change for flow trajectories outside the $f = 1$ line. Unfortunately, we are not aware of any numerical study of equation (4) for $d > 2$, so that we cannot compare predictions of our DRG flow with numerical simulations for these values of dimensionality. In any case, we expect that the numerical results obtained for $d = 1, 2$ [33] generalize for any substrate dimension. A qualitative summary of the DRG flows as obtained for different integer dimensions is provided in figure 9.

6. Discussion and conclusions

The DRG analysis of equation (4) yields a number of non-trivial results that can be classified with respect to their relevance to several issues on surface kinetic roughening: (i) the fixed point structure for a class of non-local equations, and its dependence on dimensionality, as compared to available results from numerical simulations; (ii) general consequences for stochastic equations that feature a KPZ nonlinearity, in particular the

J. Stat. Mech. (2011) P10030

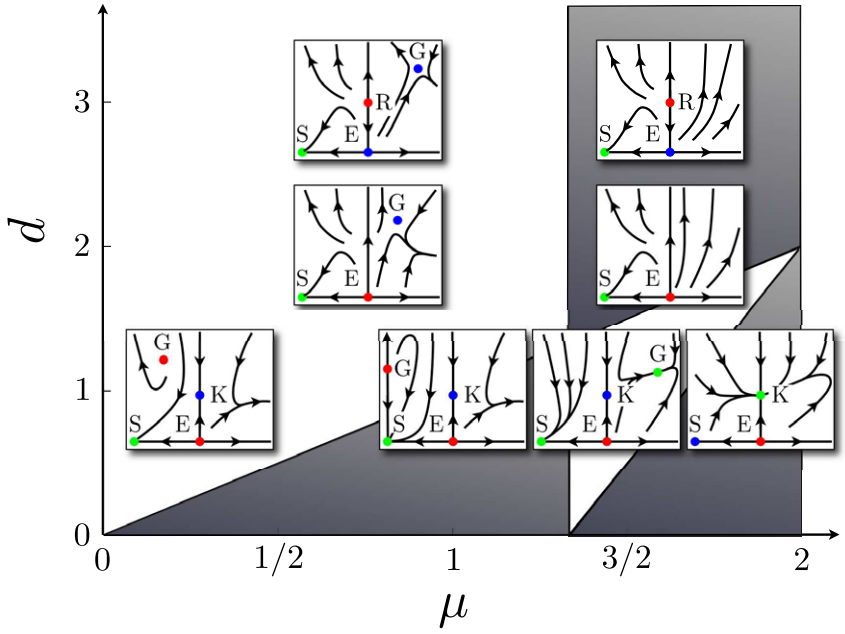

Figure 9. Qualitative behavior of the DRG flow for different values of μ and the substrate dimension d. The color of each fixed point represent its stability (red stands for unstable, blue for saddle and green for stable). The shaded region of the plane corresponds to the values of μ (as function of d) within which the Galilean fixed point is not defined.

issue of Galilean invariance; (iii) new mechanisms for the dynamical stabilization of morphologically unstable systems; (iv) the ensuing predictions on scaling behavior of realistic systems for which a continuum description can be expected to apply that fits within the framework of equation (4). We will devote this section to a brief discussion of these issues, in a way that allows us to summarize the results of the paper and put them into a wider perspective. In general, interesting new results can be anticipated from further studies of the class on non-local equations (4) along the lines discussed in the three subsections that follow.

6.1. Asymptotic properties

For different dimensions, d, our DRG analysis can be roughly summarized as a generalization of both the KPZ and the noisy Kuramoto–Sivashinsky flows, in which additional non-trivial fixed points arise that are intrinsically associated with the non-local nature of the equations that we are studying. Thus, at the Smooth and the Galilean fixed points the dynamic exponent z takes a value that coincides with the one that would be expected from a naive power counting argument, while the roughness exponent can be evaluated from the latter through a scaling relation that is either hyperscaling or the one usually associated with Galilean invariance.

The comparison between the analytical DRG results and those from numerical simulations leads to partial agreement. Specifically, in the $d = 1$ case, the change in scaling behavior that takes place for increasing μ for the morphologically stable condition [65] is described well by the DRG results. Perhaps more remarkably, the DRG seems to

also capture correctly the role of $z_{\rm KPZ}(d = 1) = 3/2$ as a critical value for μ in the morphologically unstable case, which separates asymptotic behavior between that controlled by the Galilean fixed point for $\mu < z_{\rm KPZ}(1)$ and KPZ scaling for $\mu > z_{\rm KPZ}(1)$, also in good agreement with previous numerical results [33]. However, possibly the most salient disagreement between the DRG and the numerics is the failure to generalize that role of $z_{\rm KPZ}(d)$ for general $d > 1$. This is not surprising in view of the known non-perturbative effects that are expected for the KPZ nonlinearity, particularly in higher dimensions. In general, the behavior of the Galilean fixed point changes with μ and system dimensionality in a rather non-trivial way, and some of the consequences for the DRG flow may be associated with artifacts of the perturbative scheme employed. On the other hand, the dynamic renormalization group does account for the irrelevance of higher order contributions such as those with parameter $\mathcal{N}$ in equation (4), even in the morphologically unstable case, again as observed in numerical simulations [33]. We expect that the same qualitative results apply to any equation with the shape of (9) using a general dispersion relation like (18) such that $r_1 < r_2 = 2 < \cdots < r_n$.

From a general perspective, the fact that equation (4)—and more specifically equation (19)—generalizes both the KPZ and the Lai–Das Sarma–Villain equations, has allowed us to prove vertex cancellation in the last two equations to stem merely from the shape of the nonlinearity, and to be independent of an underlying continuum symmetry of the dynamical equation. Although limited to the one loop perturbative expansion that has been employed in our DRG approach, this result may prove informative in the current questioning of Galilean invariance as inducing vertex non-renormalization in the KPZ equation, although further evidence is needed. In general, a more detailed analytical understanding of the asymptotic properties of equation (4) will require resorting to techniques that differ in nature from the perturbative DRG.

6.2. A mechanism for dynamical stabilization

A very remarkable feature of the present DRG results is that they describe analytically a mechanism for the dynamical stabilization of morphologically unstable systems, which differs from Yakhot's stabilization mechanism for the (noisy) Kuramoto–Sivashinsky equation. Namely, the latter requires renormalization of the negative 'surface tension' parameter ν to a positive value, eventually leading to asymptotic behavior in the KPZ universality class. Dynamically, as seen in numerical simulations of the noisy Kuramoto–Sivashinsky equation both in one [19, 21, 66] and in two [22] dimensions, the periodic cell structure that appears at short times is seen to evolve in a chaotic fashion that leads to height disorder and kinetic roughening properties at sufficiently long times. In marked contrast, for equation (4) the corresponding unstable ν parameter cannot change sign for $\mu < 2$, as implied by the first equation in (36), or equivalently by the fact that $f = 1$ is an invariant of the DRG flow, see equations (41)–(42). Still, the system evolves from an initial periodic morphology into a late time topography that is also disordered and rough. For any value of $\mu < 2$, this process is more similar to cell coarsening by creation and annihilation of cusps than to the familiar chaotic cell dynamics characteristic of the ($\mu = 2$) nKS case. See movies, e.g., in the Supplemental Material provided with [43] and with [33] for one and two-dimensional systems, respectively. Cusp annihilation and creation has been studied in detail in the particular case of the stochastic and deterministic Michelson–Sivashinsky equations, namely, for $\mu = 1$ with $m = 2$, see e.g. [67] and references therein,

J. Stat. Mech. (2011) P10030

but does not seem to have been studied explicitly for other values of μ. Note that, in spite of such strong differences in the dynamical evolution between the nKS equation and equation (4), they share the same KPZ asymptotic state, provided $\nu < 0$ and (as conjectured) $z_{\rm KPZ}(d) < \mu < 2$.

6.3. Comparison with experimental and other model systems

In view of the previous results on scaling properties of equation (4), a natural question concerns their experimental relevance. We believe that the kinetic roughening properties of a number of experimental systems are indeed compatible with the predictions from equation (4). For instance, in the morphologically stable condition, viscous flow induced on glassy films by ion irradiation leads to the scaling exponents obtained from (4) for $\mu = 1$ [68].

Perhaps more interestingly, a number of actual thin film systems that are characterized by large values of the growth exponent $\beta = \alpha/z$ [1] are compatible with our continuum framework in the morphologically unstable case, possibly due to the occurrence of geometrical shadowing effects [40]. For instance, in [69] Si(100) surfaces were plasma etched, finding $\alpha = 0.96 \pm 0.06$, $\beta = 0.91 \pm 0.03$ and $z = 1.05 \pm 0.09$, consistent with the predictions of equation (4) for $\mu = 1$ at the Galilean fixed point. Very similar exponent values have been recently found in chemical vapor deposition (CVD) growth of silica films [42]. CVD is an experimental technique within which shadowing instabilities are quite generically expected. Thus, e.g. in [70] amorphous hydrogenated silicon (a-Si:H) was deposited on glass via a plasma-enhanced CVD technique, finding $\beta = 1.13 \pm 0.04$ for the condition of low silane concentration in the gas mixture. Similarly, [71] reports the roughness evolution of hydrogenated amorphous carbon (a-C:H) films grown by electron cyclotron resonance CVD. A growth exponent value $\beta = 0.74$ was measured, which suggests that an underlying morphological instability is responsible for the cauliflower-like morphology observed at the late stages of the growth process, which looks quite similar to that found in [42]. Further, in [72] a large growth exponent ($\beta = 0.9 \pm 0.1$) is reported for hydrogenated diamond-like carbon (a-C:H) coatings deposited through plasma-enhanced CVD. In general, it would be interesting to search for experimental parameters/techniques that allow one to tune the value of μ, characterizing a putative continuum description through equation (4), in order to probe the corresponding continuum line of fixed points. A potential candidate might be the sticking probability in CVD systems, which seems able to tune [73] the scaling properties from KPZ-type [74] ('large' μ values) to sMS-type ($\mu = 1$) [42], although values of the effective μ parameter should be still identified that differ from $\mu = 1, 2$.

In connection with kinetic roughening in the presence of shadowing instabilities, we note that other continuum and discrete models are available [2]. Typically many of them involve the calculation of the so-called exposure angle, which is a nonlinear and non-local function of the height profile, which is very expensive to compute. By means of a small slopes expansion, the exposure angle can be seen to lead to a term of the form $kh_{\mathbf{k}}$ in the height equation [75], leading to a non-local dispersion relation as in (4) (with $\nu < 0$, $\mu = 1$, and $m = 4$). Note that for this choice of μ, the Galilean fixed point leads to the exponents $\alpha = \beta = z = 1$. However, other authors have included the non-locality of the shadowing process in the nonlinear part of the evolution equation through a non-local redistribution process of the incident particle flux [69]. The latter model has been studied numerically with a Monte Carlo method [76, 77], and analytically [78], finding the same critical

exponents, i.e., $\alpha \simeq \beta \simeq z \simeq 1$, and $\alpha = 1.04$, $\beta = 1.08$ and $z = 0.96$, respectively. In spite of the different formulation of the shadowing instability, the critical exponents coincide.

Overall, we believe that equation (4) provides a very compact description of a very wide class of systems undergoing non-conserved interface growth, both under conditions of morphological stability and in the presence of pattern forming effects. Note that, in spite of the presence of the KPZ nonlinearity in the equation of motion, KPZ scaling only occurs under the, relatively restricted, simultaneous conditions of morphological *instability* and (as conjectured) sufficiently large $\mu > z_{\rm KPZ}(d)$ values. This fact, together with the long transients induced by morphological instabilities, may account for the surprising experimental scarcity of KPZ scaling [3, 5]. Understanding the degree to which this is truly the case will require further exploration of the present and related continuum models.

Acknowledgments

We gratefully acknowledge discussions with C Escudero. This work has been partially supported through Grants Nos FIS2009-12964-C05-01 and FIS2009-12964-C05-03 (MICINN, Spain). M N acknowledges support by Fundación Carlos III (Spain) and by Fondazione Angelo Della Riccia (Italy).

Appendix A: Coarse-graining of propagator and noise variance for equation (35)

For simplicity, and as justified in more detail in appendix B, we consider equation (35), namely, equation (4) with $\sigma_{\mathbf{k}} = -\nu k^{\mu} - \mathcal{K}k^2$, as the simplest representative for the class of non-local equations studied in the main text. Here we present the detailed calculations for the coarse-graining step in the renormalization of the propagator and the noise variance for equation (35).

In equation (12) for the slow modes, the contribution from the elimination of the fast modes is contained in the function Σ. In order to evaluate expression (13), we symmetrize the wavevector integral by introducing the standard substitution $(\mathbf{q}, \Omega) \to (\mathbf{j} + \mathbf{k}/2, \Omega + \omega/2)$ [54]. We begin the calculation by considering the various contributions separately.

The wavevector contribution due to the vertex is readily obtained in the new symmetrized variables as

$$[\mathbf{q} \cdot (\mathbf{k} - \mathbf{q})][-\mathbf{q} \cdot \mathbf{k}] = j^3 \cos(\theta) k + \tfrac{1}{2} j^2 k^2 + \mathrm{O}(k^3), \tag{A.1}$$

where θ is the angle between $\mathbf{k}$ and $\mathbf{j}$. Next, we expand the contribution from the bare propagators by taking the long time limit (i.e., $\omega \to 0$),

$$\begin{aligned}
\lim_{\omega \to 0} |G_0(\hat{q})|^2 \, G_0(\hat{k} - \hat{q}) = & \left\{ \left[\nu j^{\mu} \left(1 + x\cos(\theta) + \frac{x^2}{4} \right)^{\mu/2} \right. \right. \\
& \left. \left. + \mathcal{K} j^2 \left(1 + x\cos(\theta) + \frac{x^2}{4} \right)^{\mu/2} \right]^2 + \Omega^2 \right\}^{-1} \\
& \times \left[\nu j^{\mu} \left(1 - x\cos(\theta) + \frac{x^2}{4} \right)^{\mu/2} + \mathcal{K} j^2 \left(1 - x\cos(\theta) + \frac{x^2}{4} \right)^{\mu/2} + \mathrm{i}\Omega \right]^{-1} \\
\sim & \left[1 + \left(\frac{1}{\Delta_j + \mathrm{i}z} - \frac{2\Delta_j}{\Delta_j^2 + z^2} \right) \mathcal{C}_j \cos(\theta) \frac{k}{j} \right] [(\mathcal{K} j^2)^3 (\Delta_j^2 + z^2)(\Delta_j + \mathrm{i}z)]^{-1},
\end{aligned} \tag{A.2}$$

J. Stat. Mech. (2011) P10030

where we have introduced variables $z = \Omega/\mathcal{K}j^2$ and $x = k/j$, and the function $\mathcal{C}_j = 1 + \nu\mu/2\mathcal{K}|j|^{2-\mu}$ in order to shorten the notation (Δ_j has been already defined in (39)). We can multiply the last result by (A.1) and split the integral in $\mathbf{q}$ into an angular integral in $d-1$-dimensions and a one-dimensional radial integral, where we approximate the shell to a (hyper-)spherical shape. Thus,

$$\int_> \frac{\mathrm{d}\mathbf{q}}{(2\pi)^d} = \frac{S_{d-1}}{(2\pi)^d} \int_> \mathrm{d}q\, q^{d-1} \int_0^\pi \mathrm{d}\theta\, \sin^{d-2}(\theta), \tag{A.3}$$

where $S_d = 2\pi^{d/2}/\Gamma(d/2)$ is the surface area of the d-dimensional unit sphere.

We can rewrite (13) up to second order in the external wavevector k,

$$\Sigma(\mathbf{k},0) = 2\frac{\lambda^2\Pi_0}{\mathcal{K}} \frac{S_{d-1}}{(2\pi)^{d+1}} \int_{\Lambda/b}^{\Lambda} \mathrm{d}j\, j^{d-3} \int_0^\pi \mathrm{d}\theta\, \sin^{d-2}(\theta) \times \left[j\cos(\theta) I_{11} k + \left(\tfrac{1}{2} I_{11} + \mathcal{C}_j \cos^2(\theta)\left(I_{12} - 2\Delta_j I_{21}\right)\right) k^2 \right], \tag{A.4}$$

where the integrals

$$I_{lm} = \int_{-\infty}^{+\infty} \mathrm{d}z \left(\Delta_j^2 + z^2\right)^{-l} \left(\Delta_j + \mathrm{i}z\right)^{-m}, \tag{A.5}$$

are easily calculated through the residue theorem as $I_{11} = \pi/2\Delta_j^2$, $I_{12} = \pi/4\Delta_j^3$, and $I_{21} = 3\pi/8\Delta_j^4$ (taking into account that $\Delta_j \geq 0$ for $j \in [\Lambda/b, \Lambda]$).

Integrating (A.4) in θ using

$$\int_0^\pi \mathrm{d}\theta\, \sin^{d-2}(\theta)\cos(\theta) = 0, \tag{A.6}$$

$$\int_0^\pi \mathrm{d}\theta\, \sin^{d-2}(\theta)\cos^2(\theta) = \frac{1}{d}\int_0^\pi \mathrm{d}\theta\, \sin^{d-2}(\theta), \tag{A.7}$$

$$K_d = \frac{S_{d-1}}{(2\pi)^d} \int_0^\pi \mathrm{d}\theta\, \sin^{d-2}(\theta), \tag{A.8}$$

we obtain

$$\Sigma(\mathbf{k},0) = \frac{\lambda^2\Pi_0 K_d}{4d\mathcal{K}^2} \int_{\Lambda/b}^{\Lambda} \mathrm{d}j\, \frac{j^{d-3}}{\Delta_j^3} \left(d\Delta_j - 2\mathcal{C}_j\right) k^2. \tag{A.9}$$

Finally, we perform a perturbative expansion up to first order in $1/b = \mathrm{e}^{-\delta l} = 1 - \delta l + \mathrm{O}(\delta l^2)$, which leads to

$$\Sigma(\mathbf{k},0) = \frac{\lambda^2\Pi_0 K_d}{4d} \frac{\Lambda^{d+2-2\mu}}{\left(\mathcal{K}\Lambda^{2-\mu} + \nu\right)^3} \left[(d-2)\mathcal{K}\Lambda^{2-\mu} + (d-\mu)\nu\right] \delta l\, k^2. \tag{A.10}$$

As for the coarse-graining of the noise variance, we proceed as above using the symmetrized variables,

$$\lim_{\omega\to 0} |G_0(\hat{q})|^2 \left|G_0(\hat{k}-\hat{q})\right|^2 = \frac{1}{(\mathcal{K}j^2)^4} \{[\Delta_j + \mathcal{C}_j\cos(\theta)\, x + z^2][\Delta_j - \mathcal{C}_j\cos(\theta)\, x + z^2]\}^{-1} \sim \frac{(\mathcal{K}j^2)^{-4}}{(\Delta_j^2 + z^2)^2}. \tag{A.11}$$

J. Stat. Mech. (2011) P10030

Putting this last result into the expansion of equation (17) up to zero order in powers of k, we obtain

$$\Phi(\mathbf{k},0) = \frac{\lambda^2\Pi_0^2}{(2\pi)^{d+1}}\int_{\Lambda/b}^{\Lambda} \mathrm{d}j\, j^{d-1}\int_{-\infty}^{+\infty}\mathrm{d}z\,\frac{j^4}{(\mathcal{K}j^2)^3}\frac{S_{d-1}}{(\Delta_j^2+z^2)^2}\int_0^{\pi}\mathrm{d}\theta\,\sin^{d-2}(\theta)$$
$$= \frac{\lambda^2\Pi_0^2 K_d}{4\mathcal{K}^3}\int_{\Lambda/b}^{\Lambda}\mathrm{d}j\,\frac{j^{d-3}}{\Delta_j^3} \sim \frac{\lambda^2\Pi_0^2}{4}\frac{K_d\Lambda^{d+4-3\mu}}{(\mathcal{K}\Lambda^{2-\mu}+\nu)^3}\,\delta l. \tag{A.12}$$

The modified parameters are obtained from equations (A.10) and (A.12)

$$\nu^< = \nu, \qquad \lambda^< = \lambda,$$
$$\mathcal{K}^< = \mathcal{K}\left\{1-\frac{\lambda^2\Pi_0 K_d}{4d}\frac{\Lambda^{d+2-2\mu}}{(\mathcal{K}\Lambda^{2-\mu}+\nu)^3}\left[(d-2)\mathcal{K}\Lambda^{2-\mu}+(d-\mu)\nu\right]\delta l\right\}, \tag{A.13}$$
$$\Pi_0^< = \Pi_0\left\{1+\lambda^2\Pi_0\frac{K_d\Lambda^{d+4-3\mu}}{4\,(\mathcal{K}\Lambda^{2-\mu}+\nu)^3}\delta l\right\}.$$

Now we can perform the rescaling according to the usual DRG transformation. Proceeding as indicated in the main text, the parameter flow finally reads

$$\frac{\mathrm{d}\nu}{\mathrm{d}l} = \nu\left[z-\mu\right], \qquad \frac{\mathrm{d}\lambda}{\mathrm{d}l} = \lambda\left[\alpha+z-2\right],$$
$$\frac{\mathrm{d}\mathcal{K}}{\mathrm{d}l} = \mathcal{K}\left\{z-2-\frac{\lambda^2\Pi_0 K_d}{4d}\frac{\Lambda^{d+2-2\mu}}{(\mathcal{K}\Lambda^{2-\mu}+\nu)^3}\left[(d-2)\mathcal{K}\Lambda^{2-\mu}+(d-\mu)\nu\right]\right\}, \tag{A.14}$$
$$\frac{\mathrm{d}\Pi_0}{\mathrm{d}l} = \Pi_0\left\{z-2\alpha-d+\lambda^2\Pi_0\frac{K_d\Lambda^{d+4-3\mu}}{4\,(\mathcal{K}\Lambda^{2-\mu}+\nu)^3}\right\}.$$

The set of equations (36)–(38) in the main text follows from (A.14) by imposing an unit wavevector cut-off, i.e. $\Lambda = 1$.

Appendix B: Irrelevant stabilizing terms

In this appendix we present the DRG calculations for cases of equation (4) in which the linear dispersion relation includes additional stabilizing terms (proportional to k^3 and k^4) for $1+1$ growth dimensions. We will see that the linear terms parametrized by $\mathcal{N} \neq 0$ and exponent n larger than 2 are irrelevant with respect to a term like $-k^2 h_{\mathbf{k}}$, and do not change the hydrodynamic scaling behavior of the equation. This result can be generalized straightforwardly to the full family of non-local equations considered in the main text, although for the sake of concreteness we provide the detailed DRG calculations for the case $\mu = 1$ only. This result is not surprising, since these terms are linear, and simple dimensional analysis anticipates such results. However, we have included these details for completeness, and to explicitly show how the non-trivial fixed points that control the dynamics of equation (4) already emerge when considering only the 'surface tension' term proportional to k^2, as done in sections 4 and 5, and appendix A.

To begin with, we consider a linear dispersion relation of the form

$$\sigma_k = -C_1|k| - C_2k^2 - C_3|k|^3 - C_4k^4, \tag{B.1}$$

so that in the coarse-grained propagator we have to retain powers of wavevector up to fourth order (note that here k is the one-dimensional wavevector and *not* its modulus).

J. Stat. Mech. (2011) P10030

Later on we will consider the choices $C_3 = 0$ and $C_4 = 0$ as particular cases. We proceed as in appendix A, using the standard symmetrization and considering one by one the various contributions to the integrand in equation (13). The first contribution is readily obtained as

$$k(q-k)q^2 = k\left(j+\frac{k}{2}\right)\left(j^2-\frac{k^2}{4}\right) = j^3k + \frac{1}{2}j^2k^2 - \frac{1}{4}jk^3 - \frac{1}{8}k^4. \tag{B.2}$$

The product of the first two bare propagator factors in equation (13) is evaluated considering that $|k| \ll |j|$:

$$|j+k/2| = |j| + \mathrm{sgn}(j)\, k/2, \tag{B.3}$$

$$|j+k/2|^3 = |j|^3 + 3j^2\,\mathrm{sgn}(j)\, k/2 + 3|j|k^2/4 + \mathrm{sgn}(j)\, k^3/8. \tag{B.4}$$

Using these identities, we are ready to expand the first product of two bare propagators appearing in (13) up to third order

$$\begin{aligned}\lim_{\omega\to 0}|G_0(\hat{q})|^2 &= \frac{1}{(C_4j^4)^2}\left[\left(\Delta_j + a_jx + b_jx^2 + c_jx^3\right)^2 + z^2\right]^{-1} \\ &\sim \frac{1}{(C_4j^4)^2}\frac{1}{\Delta_j^2+z^2}\left\{1 - \left(\frac{2a_j\Delta_j}{\Delta_j^2+z^2}\right)x + \frac{1}{\Delta_j^2+z^2}\left[\frac{(2a_j\Delta_j)^2}{\Delta_j^2+z^2} - 2b_j\Delta_j - a_j^2\right]x^2\right. \\ &\quad \left. + \frac{1}{\Delta_j^2+z^2}\left[\frac{4a_j\Delta_j}{\Delta_j^2+z^2}(2b_j\Delta_j + a_j^2) - 2(c_j\Delta_j + a_jb_j) - \frac{(2a_j\Delta_j)^3}{(\Delta_j^2+z^2)^2}\right]x^3\right\},\end{aligned} \tag{B.5}$$

where

$$\Delta_j = 1 + \frac{C_3}{C_4|j|} + \frac{C_2}{C_4j^2} + \frac{C_1}{C_4|j|^3}, \tag{B.6}$$

$$a_j = 2 + \frac{3}{2}\frac{C_3}{C_4|j|} + \frac{C_2}{C_4j^2} + \frac{C_1}{2C_4|j|^3}, \tag{B.7}$$

$$b_j = \frac{3}{2} + \frac{3}{4}\frac{C_3}{C_4|j|} + \frac{C_2}{4C_4j^2}, \tag{B.8}$$

$$c_j = \frac{1}{2} + \frac{C_3}{8C_4|j|}, \tag{B.9}$$

and we have introduced two new variables: the non-dimensional expansion parameter $x = k/j$, and the rescaled frequency variable $z = \Omega/(C_4j^4)$. The same procedure as applied to the remaining factor in the integrand of equation (13) leads to

$$\begin{aligned}\lim_{\omega\to 0} G_0(\hat{k}-\hat{q}) &= \frac{1}{C_4j^4}\left(\Delta_j - a_jx + b_jx^2 - c_jx^3 + \mathrm{i}z\right)^{-1} \\ &\sim \frac{1}{C_4j^4}\frac{1}{\Delta_j+\mathrm{i}z}\left\{1 + \left(\frac{a_j}{\Delta_j+\mathrm{i}z}\right)x + \frac{1}{\Delta_j+\mathrm{i}z}\left(\frac{a_j^2}{\Delta_j+\mathrm{i}z} - b_j\right)x^2\right. \\ &\quad \left. + \frac{1}{\Delta_j+\mathrm{i}z}\left[c_j - \frac{2a_jb_j}{\Delta_j+\mathrm{i}z} + \frac{a_j^3}{(\Delta_j+\mathrm{i}z)^2}\right]x^3\right\}.\end{aligned} \tag{B.10}$$

J. Stat. Mech. (2011) P10030

After multiplication of (B.5) and (B.10), we can integrate out the rescaled frequency after the change of variable $\Omega \to z = \Omega/(C_4 j^4)$. Note that the frequency integral in the new variable is

$$\int_{-\infty}^{+\infty} \mathrm{d}\Omega \to C_4 j^4 \int_{-\infty}^{+\infty} \mathrm{d}z. \tag{B.11}$$

We can use the compact notation introduced before for the integrals I_{lm} involved in the evaluation of the coarse-grained propagator (see equation (A.5)). After some algebra, we obtain the contribution to equation (13) as

$$\begin{aligned}\int_{-\infty}^{+\infty} \mathrm{d}\Omega \left| G_0\left(\hat{j}+\frac{\hat{k}}{2}\right)\right|^2 G_0\left(\frac{\hat{k}}{2}-\hat{j}\right) \sim \frac{1}{(C_4 j^4)^2}\{&I_{11} + a_j(I_{12}-2\Delta_j I_{21})x \\ &+ [a_j^2 I_{13} - b_j I_{12} - 2a_j^2\Delta_j I_{22} + (2a_j\Delta_j)^2 I_{31} - 2b_j\Delta_j I_{21} - a_j^2 I_{21}]x^2 \\ &+ [c_j I_{12} - 2a_j b_j I_{13} + a_j^3 I_{14} - 2a_j\Delta_j(a_j^2 I_{23} - b_j I_{22}) \\ &+ [(2a_j\Delta_j)^2 I_{32} - 2b_j\Delta_j I_{22} - a_j^2 I_{22}]a_j \\ &+ 4a_j\Delta_j(2b_j\Delta_j + a_j^2)I_{31} - 2(c_j\Delta_j + a_j b_j)I_{21} - (2a_j\Delta_j)^3 I_{41}]x^3\}.\end{aligned} \tag{B.12}$$

The I_{lm} integrals are easily calculated using the residue theorem, giving the contributions listed below:

$$\begin{aligned}&I_{11} = \pi/2\Delta_j^2, \quad I_{12} = \pi/4\Delta_j^3, \quad I_{13} = \pi/8\Delta_j^4, \quad I_{14} = \pi/16\Delta_j^5, \quad I_{21} = 3\pi/8\Delta_j^4, \\ &I_{22} = \pi/4\Delta_j^5, \quad I_{23} = 5\pi/32\Delta_j^6, \quad I_{31} = 5\pi/16\Delta_j^6, \\ &I_{32} = 15\pi/64\Delta_j^7, \quad I_{41} = 35\pi/128\Delta_j^8.\end{aligned}$$

Using these relation and multiplying contributions (B.2), (B.12) together, we can write Σ as the sum of four terms,

$$\Sigma(k,0) = \frac{\lambda^2\Pi_0}{4\pi}\int_{>} \mathrm{d}j\,[f_1(j)k + f_2(j)k^2 + f_3(j)k^3 + f_4(j)k^4], \tag{B.13}$$

where

$$f_1(j) = \frac{1}{(C_4\Delta_j)^2 j^5}, \qquad f_2(j) = \frac{1}{(C_4\Delta_j j^3)^2}\left(\frac{1}{2} - \frac{a_j}{\Delta_j}\right), \tag{B.14}$$

$$f_3(j) = \frac{1}{(C_4\Delta_j)^2 j^7}\left[\frac{1}{\Delta_j}\left(\frac{a_j^2}{\Delta_j} - 2b_j\right) - \frac{a_j}{2\Delta_j} - \frac{1}{4}\right], \tag{B.15}$$

$$f_4(j) = \frac{1}{(C_4\Delta_j j^4)^2}\left[\frac{1}{2\Delta_j}\left(\frac{a_j^2}{\Delta_j} - 2b_j\right) + \frac{a_j}{4\Delta_j} - \frac{1}{8} - \frac{1}{\Delta_j}\left(c_j - \frac{3}{\Delta_j}a_j b_j + \frac{a_j^3}{\Delta_j^2}\right)\right]. \tag{B.16}$$

Considering the parity of the various functions of j that appear, we can simplify expression (B.13). In fact, a_j, b_j, c_j, and Δ_j in (B.14)–(B.16) are even in j: for this reason the functions f_1 and f_3 are odd, whereas f_2 and f_4 are also even. The momentum shell is a symmetric interval around j equal to zero, hence the integrals of $f_1(j)$ and $f_3(j)$ vanish.

Another important point to address is the contribution of the shell to the renormalization of the propagator. This calculation is only required when k^4 (or higher

J. Stat. Mech. (2011) P10030

order) terms are present, because the lowest contribution from the shell occurs, precisely, at that order. Writing explicitly the integration limits in the positive part of the momentum integral, and expanding for small k [79, 80],

$$\begin{aligned}\int_{>}^{+} \mathrm{d}j\, f(j) &= \tfrac{1}{2}\left[\int_{\Lambda/b+k/2}^{\Lambda-k/2} \mathrm{d}j\, f(j) + \int_{\Lambda/b-k/2}^{\Lambda+k/2} \mathrm{d}j\, f(j)\right] \\ &\sim \int_{\Lambda/b}^{\Lambda} \mathrm{d}j\, f(j) + \frac{k}{4}\left[-f\left(\Lambda-\frac{k}{2}\right) - f\left(\frac{\Lambda}{b}+\frac{k}{2}\right)\right. \\ &\quad \left. + f\left(\Lambda+\frac{k}{2}\right) + f\left(\frac{\Lambda}{b}-\frac{k}{2}\right)\right]\Bigg|_{k=0} + \frac{k^2}{16}\left[f'\left(\Lambda-\frac{k}{2}\right) - f'\left(\frac{\Lambda}{b}+\frac{k}{2}\right)\right. \\ &\quad \left. + f'\left(\Lambda+\frac{k}{2}\right) - f'\left(\frac{\Lambda}{b}-\frac{k}{2}\right)\right]\Bigg|_{k=0} + \cdots, \end{aligned} \tag{B.17}$$

where f is any function of j (the symbol $+$ in the integral means that the integration interval is restricted to positive j). With this simple result, we see that if a function f_i in equation (B.13) contributes at order n in powers of k, then through the expansion of the shell it also contributes at every order $n+2m$, with m a positive integer. Thus, in our calculation we only need to consider the contribution of f_2 to the k^4 term as induced by the shell,

$$\int_{>}^{+} \mathrm{d}j\, f_2(j) \sim F_2(j)\Big|_{\Lambda/b}^{\Lambda} + \frac{k^2}{8}\left[f_2'(\Lambda) - f_2'(\Lambda/b)\right] \sim \left[f_2(\Lambda) + \frac{k^2}{8} f_2''(\Lambda)\right]\Lambda\delta l. \tag{B.18}$$

Here, the function F_2 is the primitive of f_2. We now introduce three new coupling variables that help us to write (B.13) in a more compact way,

$$A = \frac{C_1}{C_4|j|^3}, \qquad F = \frac{C_2}{C_4 j^2}, \qquad B = \frac{C_3}{C_4|j|}, \tag{B.19}$$

so that we can express f_2, its second derivative, and f_4 using these variables,

$$f_2(j) = -\frac{1}{2(C_4 j^3)^2}\frac{3+2B+F}{(1+A+B+F)^3}, \tag{B.20}$$

$$\begin{aligned} f_4(j) = \frac{1}{8(C_4 j^4)^4}&[11 + 40A + 27B + 29F + 2A^2 + 19B^2 + 11F^2 \\ &+ 47AB + 21AF + 35BF + (2B+F)(A^2 + 2B^2 + F^2 \\ &+ 7AB + 3AF + 4BF)](1+A+B+F)^{-5}, \end{aligned} \tag{B.21}$$

$$\begin{aligned} f_2''(j) = -\frac{1}{(C_4 j^4)^4}&[63 - 90A + 119B + 27F + 9A^2 + 82B^2 + 15F^2 - 95AB - 27AF \\ &+ 55BF + 3F^3 + 2A^2B - 3AF^2 + 20B^3 + 14BF^2 - 26AB^2 \\ &- 17ABF + 25B^2F](1+A+B+F)^{-5}. \end{aligned} \tag{B.22}$$

Considering that the shell is composed of positive and negative wavevectors, we have to count twice the previous contribution,

$$\Sigma(k,0) = \frac{\lambda^2\Pi_0}{4\pi}\left[2f_2(\Lambda)k^2 + \left(2f_4(\Lambda) + \frac{1}{4}f_2''(\Lambda)\right)k^4\right]\Lambda\delta l = \left(\Sigma_2 k^2 + \Sigma_4 k^4\right)\delta l, \tag{B.23}$$

where Σ_2 and Σ_4 are

$$\Sigma_2 = -\frac{\lambda^2\Pi_0}{4\pi}\frac{(3+2B+F)}{C_4^2\Lambda^5\,(1+A+B+F)^3}, \tag{B.24}$$

$$\begin{aligned}\Sigma_4 = -\frac{\lambda^2\Pi_0}{16\pi C_4^2\Lambda^7}[&52-130A+92B-2F+7A^2+63B^2+4F^2\\ &+16B^3+2F^3-142AB-48AF+20BF-30ABF-40AB^2-6AF^2\\ &+8BF^2-A^2F+15B^2F](1+A+B+F)^{-5}.\end{aligned} \tag{B.25}$$

In our DRG program, the next step is calculating the contributions arising from the coarse-graining of the noise variance. We start by considering equation (17) for $d = 1$. On the other hand,

$$[q(k-q)]^2 = \left(\frac{k^2}{4}-j^2\right)^2 = j^4 - \frac{1}{2}j^2k^2 + \frac{1}{16}k^4, \tag{B.26}$$

while the first factor due to the bare propagator has been already obtained, see equation (B.5). The other contribution is exactly the square of the absolute value of equation (B.10),

$$\begin{aligned}\lim_{\omega\to 0}\left|G_0\left(\frac{\hat{k}}{2}-\hat{j}\right)\right|^2 \sim \frac{(\Delta_j^2+z^2)^{-1}}{(C_4j^4)^2}\Bigg\{1+\frac{2a_j\Delta_j}{\Delta_j^2+z^2}x+\left[\frac{(2a_j\Delta_j)^2}{(\Delta_j^2+z^2)^2}-\frac{2b_j\Delta_j-a_j^2}{\Delta_j^2+z^2}\right]x^2\\ +\left[2\frac{c_j\Delta_j+a_jb_j}{\Delta_j^2+z^2}+\frac{(2a_j\Delta_j)^3}{\left(\Delta_j^2+z^2\right)^3}-\frac{4a_j\Delta_j}{(\Delta_j^2+z^2)^2}(2b_j\Delta_j+a_j^2)\right]x^3\Bigg\}.\end{aligned} \tag{B.27}$$

The coarse-graining of the non-conserved noise involves only the zeroth order term of this expansion, hence

$$\Phi(k,0) = \lambda^2\Pi_0^2\int_>\frac{\mathrm{d}j}{2\pi}\int\frac{\mathrm{d}z}{2\pi}\,j^4\left(C_4j^4\right)^{-3}\left(\Delta_j^2+z^2\right)^{-2}. \tag{B.28}$$

After integration in z, and due to the parity of the functions in (B.28), we can finally write the coarse-grained noise variance in the following form,

$$\Phi(k,0) = \frac{\lambda^2\Pi_0^2}{4\pi C_4^3}\int_{\Lambda/b}^{\Lambda}\frac{\mathrm{d}j}{j^8\Delta_j^3} = \frac{\lambda^2\Pi_0^2}{4\pi C_4^3}\frac{\delta l}{\Lambda^7\Delta_j^3}. \tag{B.29}$$

As seen in the main text, there is no renormalization for the KPZ vertex for any dispersion relation that can be written as a polynomial in k, at least within our one loop expansion. Now we are in a position to apply the usual rescaling, and to calculate the renormalized parameters

$$C_1^< = C_1, \qquad C_3^< = C_3, \tag{B.30}$$

$$C_2^< = C_2\left[1+\lambda^2\Pi_0\frac{P_2(A,B,F)}{4\pi C_2C_4^2\Lambda^5}\delta l\right], \tag{B.31}$$

$$C_4^< = C_4\left[1+\lambda^2\Pi_0\frac{P_4(A,B,F)}{16\pi C_4^3\Lambda^7}\delta l\right], \tag{B.32}$$

$$\Pi_0^< = \Pi_0\left[1+\frac{\lambda^2\Pi_0}{4\pi C_4^3}(1+A+B+F)^{-3}\frac{\delta l}{\Lambda^7}\right], \tag{B.33}$$

J. Stat. Mech. (2011) P10030

where the functions P_2 and P_4 are

$$P_2 = \frac{3+2B+F}{(1+A+B+F)^3}, \tag{B.34}$$

$$\begin{aligned} P_4 = [&52 - 130A + 92B - 2F + 7A^2 + 63B^2 + 4F^2 + 16B^3 + 2F^3 - 142AB \\ &- 48AF + 20BF - 30ABF - 40AB^2 - 6AF^2 \\ &+8BF^2 - A^2F + 15B^2F](1+A+B+F)^{-5}. \end{aligned} \tag{B.35}$$

In the next two sections we show that for a dispersion relation such as the one appearing in equation (4) with $m = 2$, additional relaxation terms with $n > 2$ do not change the hydrodynamical properties of the system as obtained in appendix A.

B.1: Irrelevance of the k^3 term

As a first case we consider the dispersion relation that is a third order polynomial in $|k|$, $\sigma_k = -C_1|k| - C_2k^2 - C_3|k|^3$. The ensuing evolution equation is an interpolation of the sMS and MSKPZ equations. Using the results already obtained, we can write the RG flow,

$$\frac{\mathrm{d}C_1}{\mathrm{d}l} = C_1[z-1], \qquad \frac{\mathrm{d}C_3}{\mathrm{d}l} = C_3[z-3], \tag{B.36}$$

$$\frac{\mathrm{d}C_2}{\mathrm{d}l} = C_2\left[z - 2 + \frac{\lambda^2\Pi_0\Lambda^2}{4\pi C_2}\left(\frac{2C_3\Lambda + C_2}{(C_1 + C_2\Lambda + C_3\Lambda^2)^3}\right)\right], \tag{B.37}$$

$$\frac{\mathrm{d}\lambda}{\mathrm{d}l} = \lambda[\alpha + z - 2], \tag{B.38}$$

$$\frac{\mathrm{d}\Pi_0}{\mathrm{d}l} = \Pi_0\left[z - 2\alpha - 1 + \frac{\lambda^2\Pi_0\Lambda^2}{4\pi}\left(C_1 + C_2\Lambda + C_3\Lambda^2\right)^{-3}\right]. \tag{B.39}$$

From equation (B.37), note that, even if the bare 'surface tension' coefficient $C_2(l=0)=0$, a non-zero value for C_2 will be generated by the RG flow, provided $C_3(l = 0) \neq 0$. Introducing the coupling variables

$$a_1 = \frac{C_1}{C_3\Lambda^2}, \qquad f_1 = \frac{C_2}{C_3\Lambda}, \qquad g_1 = \frac{\lambda^2\Pi_0}{4\pi C_3^3\Lambda^4}, \tag{B.40}$$

the resulting flow reads

$$\frac{\mathrm{d}a_1}{\mathrm{d}l} = 2a_1, \tag{B.41}$$

$$\frac{\mathrm{d}f_1}{\mathrm{d}l} = f_1\left[1 + \frac{g_1(2+f_1)}{f_1(1+a_1+f_1)^3}\right], \tag{B.42}$$

$$\frac{\mathrm{d}g_1}{\mathrm{d}l} = g_1\left[4 + \frac{g_1}{(1+a_1+f_1)^3}\right]. \tag{B.43}$$

In this case the condition $\Delta_\Lambda \geq 0$ that we have used in order to calculate the integrals I_{lm} requires $1 + a_1 + f_1 > 0$. In fact, when the dispersion relation is a third order polynomial,

J. Stat. Mech. (2011) P10030

Table B.1. Fixed point of (B.41)–(B.43) in the (a_1, f_1, g_1) space.

Name	a_1	f_1	g_1	z	α	β	λ_1	λ_2	λ_3
$\mathrm{Fp}_{3,0}$	0	0	0	3	1	1/3	2	1	4

Table B.2. Fixed point of (B.46)–(B.48) in the (a_2, f_2, g_2) space.

Name	a_2	f_2	g_2	z	α	β	λ_1	λ_2	λ_3
EW	0	0	0	2	1/2	1/4	1	−1	1
KPZ	0	0	1/2	3/2	1/2	1/3	1/2	−3/2	−1

the coefficient C_3 has to be positive and

$$\sigma_\Lambda = -C_3\Lambda^3(1 + a_1 + f_1), \tag{B.44}$$

has to be negative in order to have a well-defined short distance behavior, hence the positive sign required for the parenthesis in (B.44). For this reason we do not consider fixed points of equations (B.41)–(B.43) that do not satisfy this restriction. The only admissible fixed point in the (a_1, f_1, g_1) parameter space, $\mathrm{Fp}_{3,0}$, is reported in table B.1. This fixed point is associated with the linear limit in which $C_1 = C_2 = \lambda = 0$. All the eigenvalues of the stability matrix associated with $\mathrm{Fp}_{3,0}$ are positive, hence this fixed point is linearly unstable in every direction.

A second set of couplings that can be considered is

$$a_2 = \frac{C_1}{C_2\Lambda}, \qquad f_2 = \frac{C_3\Lambda}{C_2}, \qquad g_2 = \frac{\lambda^2\Pi_0}{4\pi C_2^3\Lambda}, \tag{B.45}$$

their flow reading

$$\frac{\mathrm{d}a_2}{\mathrm{d}l} = a_2\left[1 - \frac{g_2(2f_2+1)}{(1+a_2+f_2)^3}\right], \tag{B.46}$$

$$\frac{\mathrm{d}f_2}{\mathrm{d}l} = -f_2\left[1 + \frac{g_2(2f_2+1)}{(1+a_2+f_2)^3}\right], \tag{B.47}$$

$$\frac{\mathrm{d}g_2}{\mathrm{d}l} = g_2\left[1 - 2\frac{g_2(3f_2+1)}{(1+a_2+f_2)^3}\right]. \tag{B.48}$$

The corresponding fixed points and the eigenvalues of their stability matrices are listed in table B.2, whereby they are seen to correspond to the EW ($C_1 = C_3 = \lambda = 0$) and KPZ ($C_1 = C_3 = 0$) fixed points. Note they both have stable and unstable directions.

A third convenient set of couplings is

$$a_3 = \frac{C_3\Lambda^2}{C_1}, \qquad f_3 = \frac{C_2\Lambda}{C_1}, \qquad g_3 = \frac{\lambda^2\Pi_0\Lambda^2}{4\pi C_1^3}, \tag{B.49}$$

Table B.3. Fixed point of (B.50)–(B.52) in the (a_3, f_3, g_3) space.

Name	a_3	f_3	g_3	z	α	β	λ_1	λ_2	λ_3
Smooth	0	0	0	1	0	0	-2	-1	-2
Galilean	0	0	2	1	1	1	-2	1	2

their flow equations reading

$$\frac{\mathrm{d}a_3}{\mathrm{d}l} = -2a_3, \tag{B.50}$$

$$\frac{\mathrm{d}f_3}{\mathrm{d}l} = \frac{g_3(2a_3 + f_3)}{(1 + a_3 + f_3)^3} - f_3, \tag{B.51}$$

$$\frac{\mathrm{d}g_3}{\mathrm{d}l} = g_3 \left[\frac{g_3}{(1 + a_3 + f_3)^3} - 2 \right]. \tag{B.52}$$

In this parameter space, the Smooth and the Galilean fixed points that have been discussed in the main text arise naturally, with features as in table B.3. Note, the Smooth fixed point is completely stable in every direction.

Using the values for exponents α and z as calculated for each fixed point, we can show the irrelevance of C_3 as compared to C_2. After rescaling, equation (4) reads

$$\partial_t h_k = b^{z-1} \left[\left(-C_1|k| - \frac{C_2}{b}k^2 - \frac{C_3}{b^2}|k|^3 \right) h_k + \frac{\lambda}{2} b^{\alpha-1} \mathcal{F}\left[(\nabla h)^2\right] + b^{(1-z-2\alpha)/2}\eta_k \right], \tag{B.53}$$

and we consider now the case of $C_2, C_3 > 0$. Clearly, from linear analysis the ratio between the stabilizing terms is $C_2 b/C_3$, so that the surface tension term becomes more relevant than the $|k|^3$ term. Moreover, the sign of the eigenvalues of the linear stability matrix at the EW fixed point shows that this fixed point is stable along the direction $f_2 = C_3\Lambda/C_2$. The same situation occurs for the KPZ fixed point ($C_1 = 0$), in fact it has two negative eigenvalues associated with the two stable directions f_2 and g_2. For the Galilean fixed point, the only stable direction is $a_1 = C_3\Lambda^2/C_1$, while for the Smooth fixed point every direction is stable. The linear stability of these fixed points shows that $\mathrm{Fp}_{3,0}$ can be reached only if $C_1 = C_2 = \lambda = 0$ and is unstable in every direction, hence we can conclude that the $|k|^3$ term is irrelevant as compared to k^2 (for $C_2, C_3 > 0$). We would need this term only in the case of a negative surface tension, i.e., $C_2 < 0$, in order to have a dispersion relation that is well posed in the $k \to \infty$ limit.

B.2: Irrelevance of the k^4 term

In the last part of this appendix we show that the parameter C_4 is irrelevant when the dispersion relation contains a relaxation term with an exponent smaller than four. Let us consider a dispersion relation of the form $\sigma_k = -C_1|k| - C_2k^2 - C_4k^4$: in this case,

expressions (B.24) and (B.25) reduce to

$$\Sigma_2 = -\frac{\lambda^2\Pi_0}{4\pi C_4^2\Lambda^5}\left[\frac{3+F}{(1+A+F)^3}\right], \tag{B.54}$$

$$\Sigma_4 = -\frac{\lambda^2\Pi_0}{16\pi C_4^2\Lambda^7}[52 - 130A + 4F^2 - 2F + 2F^3 - 48AF + 7A^2 - 6AF^2 - FA^2](1+A+F)^{-5}. \tag{B.55}$$

Hence, after rescaling,

$$\frac{\mathrm{d}C_1}{\mathrm{d}l} = C_1\,[z-1]\,, \qquad \frac{\mathrm{d}\lambda}{\mathrm{d}l} = \lambda\,[\alpha+z-2] \tag{B.56}$$

$$\frac{\mathrm{d}C_2}{\mathrm{d}l} = C_2\left[z-2+\frac{\lambda^2\Pi_0\Lambda^2}{4\pi C_2}\frac{3C_4\Lambda^2+C_2}{(C_1+C_2\Lambda+C_4\Lambda^3)^3}\right], \tag{B.57}$$

$$\frac{\mathrm{d}C_4}{\mathrm{d}l} = C_4\left[z-4+\frac{\lambda^2\Pi_0}{16\pi C_4}(52C_4^3\Lambda^8 - 130C_1C_4^2\Lambda^5 - 2C_2C_4^2\Lambda^6 + 7C_1^2C_4\Lambda^2 + 4C_2^2C_4\Lambda^4 + 2C_2^3\Lambda^2 - 48C_1C_2C_4\Lambda^3 - 6C_1C_2^2\Lambda - C_1^2C_2)(C_1+C_2\Lambda+C_4\Lambda^3)^{-5}\right], \tag{B.58}$$

$$\frac{\mathrm{d}\Pi_0}{\mathrm{d}l} = \Pi_0\left[z-2\alpha-1+\frac{\lambda^2\Pi_0\Lambda^2}{4\pi}(C_1+C_2\Lambda+C_4\Lambda^3)^{-3}\right]. \tag{B.59}$$

Analogously to the result obtained in section B.1, equation (B.57) implies that, even if the bare 'surface tension' coefficient $C_2(l=0)=0$, a non-zero value will be generated for C_2 by the RG flow, provided $C_4(l=0)\neq 0$. Also in parallel to our previous computation, we consider a first set of couplings

$$a_1 = \frac{C_1}{C_4\Lambda^3}, \qquad f_1 = \frac{C_2}{C_4\Lambda^2}, \qquad g_1 = \frac{\lambda^2\Pi_0}{4\pi C_4^3\Lambda^7}, \tag{B.60}$$

for which the renormalization flow is

$$\frac{\mathrm{d}a_1}{\mathrm{d}l} = a_1\left[3-\frac{g_1}{4}(52 - 130a_1 + 4f_1^2 - 2f_1 + 2f_1^3 - 48a_1f_1 + 7a_1^2 - 6a_1f_1^2 - f_1a_1^2)(1+a_1+f_1)^{-5}\right], \tag{B.61}$$

$$\frac{\mathrm{d}f_1}{\mathrm{d}l} = 2f_1 + \frac{g_1}{4}(12 - 24f_1 + 22f_1^2 - 2f_1^4 + 24a_1 + 12a_1^2 + 56a_1f_1^2 + 162a_1f_1 - 3f_1a_1^2 + a_1^2f_1^2 + 6a_1f_1^3)(1+a_1+f_1)^{-5}, \tag{B.62}$$

$$\frac{\mathrm{d}g_1}{\mathrm{d}l} = g_1\left\{7+\frac{g_1}{(1+a_1+f_1)^3}\left[1-\frac{3}{4}(52 - 130a_1 + 4f_1^2 - 2f_1 + 2f_1^3 - 48a_1f_1 + 7a_1^2 - 6a_1f_1^2 - f_1a_1^2)(1+a_1+f_1)^{-2}\right]\right\}. \tag{B.63}$$

Table B.4. Fixed points of (B.61)–(B.63) in the (a_1, f_1, g_1) space.

Name	a_1	f_1	g_1	z	α	β
$\mathrm{Fp}_{4,0}$	0	0	0	4	3/2	3/8
KPZ	0	13.1868	1064.4	1.54	0.46	0.299
$\mathrm{Fp}_{4,1}$	7.17	−6	20.4	1	1	1

Table B.5. Eigenvalues of the fixed points of table B.4.

Name	λ_1	λ_2	λ_3	Stability
$\mathrm{Fp}_{4,0}$	3	2	7	Unstable
KPZ	0.54	−2.90	−1.06	Saddle
$\mathrm{Fp}_{4,1}$	88.4	7.33	−0.24	Saddle

The different fixed points in the (a_1, f_1, g_1) parameter space are given in table B.4, where the coordinates of the KPZ fixed point have been determined using the only admissible real solution, x_0, of equation $x^4 - 8x^3 - 63x^2 - 68x - 42 = 0$. Hence, the KPZ fixed point is located at the point $(0, x_0, P(x_0))$, where $P(x) = (686 + 969x + 846x^2 - 25x^3)/97$. Likewise, the $\mathrm{Fp}_{4,1}$ fixed point has been obtained solving $7y^2 + 2y - 374 = 0$ and using the only admissible solution y_0 for the components of vector $(y_0, -6, Q(y_0))$, where $Q(y) = (13\,014y - 92\,286)/49$. The $\mathrm{Fp}_{4,0}$ fixed point is associated with the linear molecular beam epitaxy (MBE) equation ($C_1 = C_2 = \lambda = 0$) [1], while $\mathrm{Fp}_{4,1}$ has the same exponents as (but does not coincide with) the Galilean fixed point. The stability matrices of these points are dense, and we report their eigenvalues in table B.5. All these points are unstable, or at least hyperbolic, in the three-dimensional space, but if we consider the $C_1 = 0$ plane, the KPZ fixed point is stable.

A second set of couplings is provided by

$$a_2 = \frac{C_1}{C_2\Lambda}, \qquad f_2 = \frac{C_4\Lambda^2}{C_2}, \qquad g_2 = \frac{\lambda^2\Pi_0}{4\pi C_2^3\Lambda}, \tag{B.64}$$

whose flow is

$$\frac{\mathrm{d}a_2}{\mathrm{d}l} = a_2\left[1 - \frac{g_2(1+3f_2)}{(1+a_2+f_2)^3}\right], \tag{B.65}$$

$$\frac{\mathrm{d}f_2}{\mathrm{d}l} = f_2\left[\frac{g_2}{4f_2}(2 - 12f_2^4 + 24f_2^3 - 162a_2f_2^2 - 22f_2^2 - 56a_2f_2 - 6a_2 - a_2^2 - 12a_2^2f_2^2 - 24a_2f_2^3)(1+a_2+f_2)^{-5} - 2\right], \tag{B.66}$$

$$\frac{\mathrm{d}g_2}{\mathrm{d}l} = g_2\left[1 - \frac{g_2(2+9f_2)}{(1+a_2+f_2)^3}\right]. \tag{B.67}$$

We provide the ensuing fixed points in table B.6 (note they include the EW and KPZ fixed points), while their stability properties are given in table B.7.

J. Stat. Mech. (2011) P10030

Table B.6. Fixed points of (B.65)–(B.67) in the (a_2, f_2, g_2) space.

Name	a_2	f_2	g_2	z	α	β
EW	0	0	0	2	1/2	1/4
KPZ	0	0.075 83	0.4642	1.54	0.46	0.299
$\mathrm{Fp}_{4,1}$	−1.1946	−1/6	−0.094 36	1	1	1

Table B.7. Eigenvalues of the fixed points of table B.6.

Name	λ_1	λ_2	λ_3	Stability
EW	1	−2	1	Saddle
KPZ	0.54	−2.90	−1.05	Saddle
$\mathrm{Fp}_{4,1}$	88.4	7.32	−0.24	Saddle

Table B.8. Fixed points of (B.69)–(B.71) in the (a_3, f_3, g_3) space.

Name	a_1	f_1	g_1	z	α	β
Smooth	0	0	0	1	0	0
Galilean	0	0	2	1	1	1
$\mathrm{Fp}_{4,1}$	0.1395	−0.8371	0.055 34	1	1	1

Table B.9. Eigenvalues of the fixed points of table B.8.

Name	λ_1	λ_2	λ_3	Stability
Smooth	−1	−3	−2	Stable
Galilean	2	$\frac{3}{4} + \mathrm{i}\frac{\sqrt{47}}{4}$	$\frac{3}{4} + \mathrm{i}\frac{\sqrt{47}}{4}$	Unstable
$\mathrm{Fp}_{4,1}$	1.09	2.28	−1.98	Saddle

Finally, a further informative set of coupling parameters is

$$a_3 = \frac{C_4\Lambda^3}{C_1}, \qquad f_3 = \frac{C_2\Lambda}{C_1}, \qquad g_3 = \frac{\lambda^2\Pi_0\Lambda^2}{4\pi C_1^3}, \tag{B.68}$$

whose flow is

$$\frac{\mathrm{d}a_3}{\mathrm{d}l} = -3a_3 + \frac{g_3}{4}[52a_3^3 - 2f_3a_3^2 + 4f_3^2a_3 + 2f_3^3 - 130a_3^2 - 48a_3f_3 + 7a_3 - 6f_3^2 - f_3](1 + a_3 + f_3)^{-5}, \tag{B.69}$$

$$\frac{\mathrm{d}f_3}{\mathrm{d}l} = -f_3 + \frac{g_3(3a_3 + f_3)}{(1 + a_3 + f_3)^3}, \tag{B.70}$$

$$\frac{\mathrm{d}g_3}{\mathrm{d}l} = g_3\left[\frac{g_3}{(1 + a_3 + f_3)^3} - 2\right]. \tag{B.71}$$

In this parameter space the fixed points and their exponents are in table B.8, and the associated eigenvalues in table B.9. The $\mathrm{Fp}_{4,1}$ fixed point is obtained by solving equation

$374x^2 - 2x - 7 = 0$ and using the only admissible solution $x_1 = (1 + \sqrt{291})/374$ for the components of vector $(x_1, -6x_1, L(x_1))$, where $L(x) = (167\,238 - 1184\,895x)/34\,969$.

As done for the $|k|^3$ term, we can show the irrelevance of the k^4 'surface diffusion' term, compared to the k^2 'surface tension' one for $C_2, C_4 > 0$. After rescaling of equation (4), the ratio between these two terms is equal to $C_2 b^2/C_4$. In the presence of surface diffusion, we obtain several fixed points which are not present in its absence. However, the only fixed point with exponents different from those found in section 4 is $\mathrm{Fp}_{4,0}$, i.e. the linear MBE fixed point, while $\mathrm{Fp}_{4,1}$ has the same exponents as the Galilean fixed point, $z = 1$ and $\alpha = 1$. The stability matrices show the latter fixed point has one stable direction, while the Galilean and $\mathrm{Fp}_{4,0}$ fixed points are both unstable. The KPZ fixed point has two stable directions and becomes the only stable fixed point of the DRG flow if we restrict our analysis to the $C_1 = 0$ case, i.e. $a_4 = 0$. Finally, as for the $|k|^3$ term, surface diffusion does not introduce any unexpected behavior in the case $C_1 \neq 0$ and $C_2 > 0$, hence we conclude that the C_4 term is required only when $C_2 < 0$, in order to have a dispersion relation that is well posed in the $k \to \infty$ limit.

In summary, within the limitations of the DRG technique, we have shown that the main conclusions obtained for a linear dispersion relation of the $|k| - k^2$ type also apply in the presence of higher order polynomial contributions, as long as they have the proper stabilizing signs. Only when the k^2 surface tension term is destabilizing are such higher order terms required for physical consistency. A similar conclusion is expected for $\mu \neq 1$ values. This irrelevance (and also the self-consistency of the DRG calculations) qualifies equation (35) as a faithful representative of the scaling behavior of (4), as employed in the main text.

References

[1] Barabási A-L and Stanley H E, 1995 *Fractal Concepts in Surface Growth* (Cambridge: Cambridge University Press)
[2] Krug J, 1997 *Adv. Phys.* **46** 139
[3] Cuerno R, Castro M, Muñoz-García J, Gago R and Vázquez L, 2007 *Eur. Phys. J. Spec. Top.* **146** 427
[4] Misbah C, Pierre-Louis O and Saito Y, 2010 *Rev. Mod. Phys.* **82** 981
[5] Cuerno R and Castro M, 2001 *Phys. Rev. Lett.* **87** 236103
[6] Nicoli M, Castro M and Cuerno R, 2008 *Phys. Rev.* E **78** 021601
[7] Krug J and Meakin P, 1991 *Phys. Rev. Lett.* **66** 703
[8] Biler P, Karch G and Woyczynski W A, 1999 *Studia Math.* **135** 231
[9] Cross M and Greenside H, 2009 *Pattern Formation and Dynamics in Nonequilibrium Systems* (Cambridge: Cambridge University Press)
[10] Pelcé P, 2004 *New Visions on Form and Growth* (New York: Oxford University Press)
[11] Saffman P G and Taylor G, 1958 *Proc. R. Soc. London* A **245** 312
[12] Bensimon D, Kadanoff L P, Liang S, Shraiman B I and Tang C, 1986 *Rev. Mod. Phys.* **58** 977
[13] Darrieus G, 1938 unpublished
[14] Landau L D, 1944 *Acta Physicochim. URSS* **19** 77
[15] Clanet C and Searby G, 1998 *Phys. Rev. Lett.* **80** 3867
[16] Bychkov V V and Liberman M A, 2000 *Phys. Rep.* **325** 115
[17] Kardar M, Parisi G and Zhang Y-C, 1986 *Phys. Rev. Lett.* **56** 889
[18] Castro M, Muñoz-García J, Cuerno R, García Hernández M M and Vázquez L, 2007 *New J. Phys.* **9** 102
[19] Cuerno R, Makse H A, Tomassone S, Harrington S T and Stanley H E, 1995 *Phys. Rev. Lett.* **75** 4464
[20] Cuerno R and Lauritsen K B, 1995 *Phys. Rev.* E **52** 4853
[21] Ueno K, Sakaguchi H and Okamura M, 2005 *Phys. Rev.* E **71** 046138
[22] Nicoli M, Vivo E and Cuerno R, 2010 *Phys. Rev.* E **82** 045202
[23] Pradas M, Tseluiko D, Kalliadasis S, Papageorgiou D T and Pavliotis G A, 2011 *Phys. Rev. Lett.* **106** 060602
[24] Yakhot V, 1981 *Phys. Rev.* A **24** 642

J. Stat. Mech. (2011) P10030

[25] McComb W D, 1991 *The Physics of Fluid Turbulence* (New York: Oxford University Press)
[26] Halpin-Healy T and Zhang Y-C, 1995 *Phys. Rep.* **254** 215
[27] Medina E, Hwa T, Kardar M and Zhang Y-C, 1989 *Phys. Rev.* A **39** 3053
[28] Cuerno R and Vázquez L, 2004 *Advanced in Condensed Matter and Statistical Physics* ed E Korutcheva and R Cuerno, Nova Science Publishers, p 237
[29] Tang G and Ma B, 2001 *Physica* A **298** 257
[30] Mann J A and Woyczynski W A, 2001 *Physica* A **291** 159
[31] Katzav E, 2003 *Phys. Rev.* E **68** 031607
[32] Cuerno R and Castro M, 2002 *Physica* A **314** 192
[33] Nicoli M, Cuerno R and Castro M, 2009 *Phys. Rev. Lett.* **102** 256102
[34] Samko S G, Kilbas A A and Marichev O I, 2002 *Fractional Integrals and Derivatives* (London: Taylor and Francis)
[35] Silvestre L, 2007 *Commun. Pure Appl. Math.* **60** 0067
[36] Mukamel D, 2008 *Proc. of the Les Houches Summer School on Long-Range Interacting Systems* (New York: Elsevier)
[37] Kim D H and Kim J M, 2010 *J. Stat. Mech.* P08008
[38] Sivashinsky G I, 1977 *Acta Astronaut.* **4** 1177
[39] Michelson D M and Sivashinsky G I, 1977 *Acta Astronaut.* **4** 1207
[40] Bales G S, Bruinsma R, Eklund E, Karunasiri R, Rudnick J and Zangwill A, 1990 *Science* **249** 264
[41] Kechagia P, Yortsos Y C and Lichtner P, 2001 *Phys. Rev.* E **64** 016315
[42] Castro M, Buijnsters I, Nicoli M, Cuerno R and Vázquez L, 2011 unpublished
[43] Nicoli M, Castro M and Cuerno R, 2009 *J. Stat. Mech.* P02036
[44] Haselwandter C A and Vvedensky D D, 2007 *Phys. Rev. Lett.* **98** 046102
[45] Haselwandter C A and Vvedensky D D, 2010 *Phys. Rev.* E **81** 021606
[46] Keller A, Nicoli M, Facsko S and Cuerno R, 2011 *Phys. Rev.* E **84** 015202
[47] Lai Z-W and Das Sarma S, 1991 *Phys. Rev. Lett.* **66** 2348
[48] Villain J, 1991 *J. Physique* I **1** 19
[49] Hentschel H G E and Family F, 1991 *Phys. Rev. Lett.* **66** 1982
[50] Kardar M, 2007 *Statistical Physics of Fields* (Cambridge: Cambridge University Press)
[51] Fisher M E, Ma S-K and Nickel B G, 1972 *Phys. Rev. Lett.* **29** 917
[52] Giada L, Giacometti A and Rossi M, 2002 *Phys. Rev.* E **65** 036134
[53] Gallego R, Castro M and López J M, 2007 *Phys. Rev.* E **76** 051121
[54] Forster D, Nelson D R and Stephen M J, 1977 *Phys. Rev.* A **16** 732
[55] Lauritsen K B, 1995 *Phys. Rev.* E **52** R1261
[56] Janssen H K, 1997 *Phys. Rev. Lett.* **78** 1082
[57] Frey E and Täuber U C, 1994 *Phys. Rev.* E **50** 1024
[58] Sun T and Plischke M, 1994 *Phys. Rev.* E **49** 5046
[59] McComb W D, 2005 *Phys. Rev.* E **71** 037301
[60] Berera A and Hochberg D, 2007 *Phys. Rev. Lett.* **99** 254501
[61] Berera A and Hochberg D, 2009 *Nucl. Phys.* B **814** 522
[62] Wio H S, Revelli J A, Deza R R, Escudero C and de la Lama M S, 2010 *Europhys. Lett.* **89** 40008
[63] Wio H S, Escudero C, Revelli J A, Deza R R and de la Lama M S, 2011 *Phil. Trans. R. Soc.* A **369** 396
[64] Marinari E, Pagnani A and Parisi G, 2000 *J. Phys. A: Math. Gen.* **33** 8181
[65] Nicoli M, Cuerno R and Castro M, 2011 unpublished
[66] Karma A and Misbah C, 1993 *Phys. Rev. Lett.* **71** 3810
[67] Kupervasser O and Olami Z, 2011 arXiv:1106.0558v1
[68] Mayr S G and Averback R S, 2001 *Phys. Rev. Lett.* **87** 196106
[69] Zhao Y-P, Drotar J T, Wang G-C and Lu T-M, 1999 *Phys. Rev. Lett.* **82** 4882
[70] Dalakos G T, Plawsky J P and Persans P D, 2005 *Phys. Rev.* B **72** 205305
[71] Buijnsters J G and Vázquez L, 2008 *J. Phys. D: Appl. Phys.* **41** 012006
[72] Hormann C, Meier S and Moseler M, 2009 *Eur. Phys. J.* B **69** 187
[73] Castro M, Cuerno R, Sánchez A and Domínguez-Adame F, 2000 *Phys. Rev.* E **62** 161
[74] Ojeda F, Cuerno R, Salvarezza R and Vázquez L, 2000 *Phys. Rev. Lett.* **84** 3125
[75] Karunasiri R P U, Bruinsma R and Rudnick J, 1989 *Phys. Rev. Lett.* **62** 788
[76] Drotar J T, Zhao Y-P, Lu T-M and Wang G-C, 2000 *Phys. Rev.* B **61** 3012
[77] Drotar J T, Zhao Y-P, Lu T-M and Wang G-C, 2000 *Phys. Rev.* B **62** 2118
[78] Chattopadhyay A K, 2002 *Phys. Rev.* B **65** 041405
[79] Alonso-Sánchez F and Hochberg D, 2000 *Phys. Rev.* E **62** 7008
[80] Berera A and Yoffe S R, 2010 *Phys. Rev.* E **82** 066304

J. Stat. Mech. (2011) P10030